Charm photoproduction at HERA: k_T-factorization versus experimental data

A.V. Lipatov, N.P. Zotov

November 24, 2006

D.V. Skobeltsyn Institute of Nuclear Physics,
M.V. Lomonosov Moscow State University,
119992 Moscow, Russia

Abstract

We calculate the cross section of charm photoproduction at HERA collider in the framework of the k_T-factorization QCD approach. Our analysis cover the inclusive charm production as well as charm and associated jet production processes. Both photon-gluon and gluon-gluon fusion mechanisms are taken into account. The unintegrated gluon densities in a proton and in a photon obtained from the full CCFM, from unified BFKL-DGLAP evolution equations as well as from the Kimber-Martin-Ryskin prescription are used. Our theoretical results are compared with the recent experimental data taken by the H1 and ZEUS collaborations at HERA. Special attention is put on the specific angular correlations which can provide unique information about non-collinear gluon evolution dynamics.

1 Introduction

The charmed quark production in electron-proton collisions at HERA is a subject of intensive study from both theoretical and experimental points of view [1–6]. The value of charm mass m_c provides a hard scale which allows perturbative QCD (pQCD) to be applied. The production dynamics is governed by the photon-gluon $\gamma g \to c\bar{c}$ or gluon-gluon fusion $gg \to c\bar{c}$ (direct and resolved photon contributions, respectively) and therefore cross sections of such processes are sensitive to the gluon content of a proton and of a photon. Very recently, the H1 and ZEUS collaborations have presented important experimental data [5, 6] on the charm photoproduction at HERA. In [6] the data sample five times larger than in previous analysis [1] has been used. Differential cross sections are determined for events with a $D^{*\pm}$ meson (inclusive $D^{*\pm}$ production) and for events with a $D^{*\pm}$ meson and one

or two hadronic jets. In the ZEUS analysis [5] the differential inclusive jet cross sections for events containing a $D^{*\pm}$ meson have been measured and specific angular correlations in the $D^{*\pm}$ and dijet associated photoproduction have been studied. A comparison of these measurements with the next-to-leading (NLO) pQCD calculations shows [5, 6] that NLO pQCD has some marked problems in description of experimental data. In particular, the significant differences are observed [5] in the shape and in the normalization of most of the distributions between data and theoretical predictions. On the other hand recently much progress has been made towards a global understanding of the k_T-factorization [7, 8] (or semihard [9, 10]) approach by working out this picture for several heavy quark and prompt photon production processes at HERA and Tevatron [11–15].

The k_T-factorization approach is based on the familiar Balitsky-Fadin-Kuraev-Lipatov (BFKL) [16] or Ciafaloni-Catani-Fiorani-Marchesini (CCFM) [17] gluon evolution. In this way, the large logarithmic terms proportional to $\ln 1/x$ are summed up to all orders of perturbation theory (in the leading logarithmic approximation). It is in contrast with the popular Dokshitzer-Gribov-Lipatov-Altarelli-Parizi (DGLAP) [18] strategy where only large logarithmic terms proportional to $\ln \mu^2$ are taken into account. The basic dynamical quantity of the k_T-factorization approach is the so-called unintegrated (i.e. $\mathbf{k}_T$-dependent) gluon distribution $\mathcal{A}(x, \mathbf{k}_T^2, \mu^2)$ which determines the probability to find a gluon carrying the longitudinal momentum fraction x and the transverse momentum $\mathbf{k}_T$ at the probing scale μ^2. The unintegrated gluon distribution can be obtained from the analytical or numerical solution of the BFKL or CCFM evolution equations. Similar to DGLAP, to calculate the cross sections of any physical process the unintegrated gluon density $\mathcal{A}(x, \mathbf{k}_T^2, \mu^2)$ has to be convoluted [7–10] with the relevant partonic cross section. But as the virtualities of the propagating gluons are no longer ordered, the partonic cross section has to be taken off mass shell ($\mathbf{k}_T$-dependent). It is in clear contrast with the usual DGLAP scheme (so-called collinear factorization). Since gluons in the initial state are not on-shell and are characterized by virtual masses (proportional to their transverse momentum), it also assumes a modification of their polarization density matrix [7, 8]. In particular, the polarization vector of a gluon is no longer purely transversal, but acquires an admixture of longitudinal and time-like components. Other important properties of the k_T-factorization formalism are the additional contribution to the cross sections due to the integration over the $\mathbf{k}_T^2$ region above μ^2 and the broadening of the transverse momentum distributions due to extra transverse momentum of the colliding partons.

Concerning the theoretical treatment of charm production in the framework of standard (collinear) QCD, two types of NLO calculations are available for comparison with the recent H1 and ZEUS experimental data [5, 6]. The traditional massive charm approach [19] or fixed-flavour-number scheme (FFNS) assumes that light quarks are the only active flavours in the structure functions of the proton and photon, so that charmed quarks are produced only in the hard process. This scheme should be reliable when the transverse momentum p_T of the charmed quarks is of similar size compared to m_c and breaks down for $p_T \gg m_c$. It is because of presence of collinear singularities which having the form $\alpha_s \ln(p_T^2/m_c^2)$. In the massless or zero-mass variable-flavour-number scheme (ZMVFNS) [20] charmed quarks are treated as an additional active flavours (massless partons). This approach is applicable at high transverse momenta $p_T \gg m_c$. To completeness, we should also mention the general-mass variable-flavour-number scheme (GMVFNS) [21] which combines the massless and

the massive scheme. Note that the massless charm calculations take into account charm excitation processes and thus predict a larger resolved component in comparison with the massive calculations. However, both massless and massive approaches underestimate [6] the measured cross section of the inclusive $D^{*\pm}$ photoproduction in the intermediate transverse momentum p_T and forward pseudo-rapidity η regions. An agreement between the theoretical and experimental results can only be achieved using some extreme parameter values. In particular, in the NLO massive scheme a very low charmed quark mass $m_c = 1.2$ GeV was required [19]. But even within this set of parameters, the shapes of the $D^{*\pm}$ transverse momentum and pseudo-rapidity distributions cannot be said well reproduced. Some better agreement between the massless scheme and the measured p_T (though not η) spectrum was achieved using special assumptions on the $c \to D^*$ fragmentation. The similar situation is observed in the case of semi-inclusive charm production: the data tends to agree with the upper bound of the NLO calculation [5]. However, the difference between the results of NLO calculation observed in shape of inclusive differential cross section as function of the pseudo-rapidity $\eta_{D^{*\pm}}$ is not seen in the semi-inclusive cross section as a function of $\eta^{\rm jet}$, and the shape of the data is well described by the NLO QCD predictions. At the same time the experimentally obtained dijet angular correlations [5] show a large deviation from the massive NLO QCD predictions, specially for the resolved-enriched sample. In general, it was concluded [6] that for the precise description of the charm photoproduction higher-order corrections or implementation of additional parton showers in current NLO calculations are needed.

In our previous paper [11] the ability of the k_T-factorization approach to reproduce the recent experimental data for the $D^{*\pm}$ and dijet associated photoproduction (including the specific angular correlations between the hadronic jets in final state) taken by the ZEUS collaboration has been investigated. It was demonstrated [11, 22, 23] that the leading-order off-shell matrix elements of the photon-gluon fusion $|\bar{\mathcal{M}}|^2(\gamma g^* \to c\bar{c})$ combined with the non-collinear evolution of gluon densities in a proton $\mathcal{A}(x, \mathbf{k}_T^2, \mu^2)$ effectively simulate contribution from the charmed quark excitation subprocess $cg \to cg$. Next, some $c - \bar{c}$ correlations in high energy γp scattering have been studied [24] and comparisons to the recently measured data of the FOCUS collaboration at Fermilab were made. In particular, it was shown that the analysis of the kinematical correlations of charmed quarks opens new possibilities for verifying models of non-collinear gluon evolution.

In the present paper we will analyse the recent H1 and ZEUS data [5, 6] using the k_T-factorization approach of QCD. Mostly we will concentrate on the $D^{*\pm}$ and single jet associated photoproduction. It is because these processes have not been studied yet in the framework of k_T-factorization and the comparison to the experimental data [6] were made in the framework of MC generator CASCADE [25] only. We investigate the different production rates (calculated in a number of different kinematical regions) and make a systematic comparison of our predictions to the recent H1 and ZEUS data. Special attention will be drawn to the specific angular correlations in associated $D^{*\pm}$ and jet production since these correlations are sensitive to the transverse momentum of the partons incoming to the hard scattering process and therefore sensitive to the details of the non-collinear gluon evolution. Additional motivation of this study is the fact that k_T-factorization approach automatically incorporates the main part of the standard (collinear) high-order corrections [7–10]. Our consideration will be based on the leading-order off-shell matrix elements of the photon-

gluon and gluon-gluon fusion subprocesses (the direct and resolved photon contributions, respectively) which have been calculated in our previous papers [12, 26]. In the numerical calculations we will test the different sets of unintegrated gluon distributions in a proton and in a photon which are obtained from the full CCFM [27], from the unified BFKL-DGLAP evolution equations [28] and from the conventional (DGLAP-based) quark and gluon densities. In the last case we will use the so-called Kimber-Martin-Ryskin (KMR) [29] approach.

The outline of our paper is following. In Section 2 we recall shortly the basic formulas of the k_T-factorization approach with a brief review of calculation steps. In Section 3 we present the numerical results of our calculations and a discussion. Finally, in Section 4, we give some conclusions.

2 Theoretical framework

2.1 Kinematics

We start from the gluon-gluon fusion subprocess. Let p_e and p_p be the four-momenta of the initial electron and proton, k_1 and k_2 the four-momenta of the incoming off-shell gluons, and p_c and $p_{\bar{c}}$ the four-momenta of the produced charmed quarks. In our analysis below we will use the Sudakov decomposition, which has the following form:

$$\begin{aligned} p_c = \alpha_1 p_e + \beta_1 p_p + p_{cT}, \quad p_{\bar{c}} = \alpha_2 p_e + \beta_2 p_p + p_{\bar{c}T}, \\ k_1 = x_1 p_e + k_{1T}, \quad k_2 = x_2 p_p + k_{2T}, \end{aligned} \tag{1}$$

where k_{1T}, k_{2T}, p_{cT} and $p_{\bar{c}T}$ are the transverse four-momenta of the corresponding particles. It is important that $\mathbf{k}_{1T}^2 = -k_{1T}^2 \neq 0$ and $\mathbf{k}_{2T}^2 = -k_{2T}^2 \neq 0$. If we make replacement $k_1 \to p_e$ and set $x_1 = 1$ and $k_{1T} = 0$, then we easily obtain more simpler formulas corresponding to photon-gluon fusion subprocess. In the ep center-of-mass frame we can write

$$p_e = \sqrt{s}/2(1,0,0,1), \quad p_p = \sqrt{s}/2(1,0,0,-1), \tag{2}$$

where $s = (p_e + p_p)^2$ is the total energy of the process under consideration and we neglect the masses of the incoming particles. The Sudakov variables are expressed as follows:

$$\begin{aligned} \alpha_1 = \frac{m_{cT}}{\sqrt{s}} \exp(y_c), \quad \alpha_2 = \frac{m_{\bar{c}T}}{\sqrt{s}} \exp(y_{\bar{c}}), \\ \beta_1 = \frac{m_{cT}}{\sqrt{s}} \exp(-y_c), \quad \beta_2 = \frac{m_{\bar{c}T}}{\sqrt{s}} \exp(-y_{\bar{c}}), \end{aligned} \tag{3}$$

where m_{cT} and $m_{\bar{c}T}$ are the transverse masses of the produced quarks, and y_c and $y_{\bar{c}}$ are their rapidities (in the ep center-of-mass frame). From the conservation laws we can easily obtain the following conditions:

$$x_1 = \alpha_1 + \alpha_2, \quad x_2 = \beta_1 + \beta_2, \quad \mathbf{k}_{1T} + \mathbf{k}_{2T} = \mathbf{p}_{cT} + \mathbf{p}_{\bar{c}T}. \tag{4}$$

In order to be sensitive to higher-order effects and to distinguish between direct-enriched and resolved-enriched regions the variable $x_\gamma^{\rm obs}$ is often used [5] in the analysis of the data which contain the jets. This variable, which is the fraction of the photon momentum contributing

to the production of two jets with highest transverse energies $E_T^{\rm jet}$, is experimentally defined as

$$x_\gamma^{\rm obs} = \frac{E_T^{{\rm jet}_1} e^{-\eta^{{\rm jet}_1}} + E_T^{{\rm jet}_2} e^{-\eta^{{\rm jet}_2}}}{2yE_e}, \tag{5}$$

where yE_e is the initial photon energy and $\eta^{{\rm jet}_i}$ are the pseudo-rapidities of these hardest jets. The pseudo-rapidities $\eta^{{\rm jet}_i}$ are defined as $\eta^{{\rm jet}_i} = -\ln\tan(\theta^{{\rm jet}_i}/2)$, where $\theta^{{\rm jet}_i}$ are the polar angles of the jets with respect to the proton beam. The selection of $x_\gamma^{\rm obs} > 0.75$ and $x_\gamma^{\rm obs} < 0.75$ yields samples enriched in direct and resolved photon processes, respectively. Another interesting variables, namely $x_\gamma^{\rm obs}(D^*)$ and $\cos\theta^*$, are also often used [5, 6] in the analysis of the experimental data. The $x_\gamma^{\rm obs}(D^*)$ variable can be constructed in an analogous way to the traditional $x_\gamma^{\rm obs}$ [5]. Using the $D^{*\pm}$ meson and the untagged jet (i.e. jet which is not matched to a $D^{*\pm}$ meson) of highest $E_T^{\rm jet}$, the quantity $x_\gamma^{\rm obs}(D^*)$ is given by

$$x_\gamma^{\rm obs}(D^*) = \frac{p_T e^{-\eta} + E_T^{\rm jet} e^{-\eta^{\rm jet}}}{2yE_e}, \tag{5}$$

where p_T and η are the transverse momentum and pseudo-rapidity of the produced $D^{*\pm}$ meson. The scattering angle θ^* is defined as

$$\cos\theta^* = \tanh\frac{\eta - \eta^{\rm jet}}{2}. \tag{11}$$

Studying the distribution of $\cos\theta^*$ also gives us the possibility to learn about the size of the contributions from different production mechanisms [5]. Finally, the inelasticity z, defined by $z = (p_p \cdot p)/(p_p \cdot q)$ with p and q being the four-momenta of the final $D^{*\pm}$ meson and the exchanged photon, is a measure of the fraction of photon energy transferred to the $D^{*\pm}$ meson in the proton rest frame. This quantity is sensitive to both the production mechanism and to the $c \to D^*$ fragmentation details [6].

2.2 Cross section for charm photoproduction

The main formulas for the total and differential cross sections for charm production cross sections were obtained in our previous papers [11, 12, 26]. Here we recall some of them. In general case, the cross section σ according to k_T-factorization theorem can be written as a convolution

$$\sigma = \int d\mathbf{k}_T^2\, \hat{\sigma}(\mathbf{k}_T^2, \mu^2) \mathcal{A}(x, \mathbf{k}_T^2, \mu^2), \tag{6}$$

where $\hat{\sigma}(\mathbf{k}_T^2, \mu^2)$ is the cross section corresponding to the relevant partonic subprocess under consideration and $\mathcal{A}(x, \mathbf{k}_T^2, \mu^2)$ is the unintegrated gluon distribution. The direct photon contribution to the differential cross section of $\gamma p \to c\bar{c} + X$ process is given by

$$\frac{d\sigma^{(\rm dir)}(\gamma p \to c\bar{c} + X)}{dy_c\, d\mathbf{p}_{cT}^2} = \int \frac{|\bar{\mathcal{M}}|^2(\gamma g^* \to c\bar{c})}{16\pi (x_2 s)^2 (1-\alpha_1)} \mathcal{A}(x_2, \mathbf{k}_{2T}^2, \mu^2) d\mathbf{k}_{2T}^2 \frac{d\phi_2}{2\pi} \frac{d\phi_c}{2\pi}, \tag{7}$$

where $|\bar{\mathcal{M}}|^2(\gamma g^* \to c\bar{c})$ is the squared off-shell matrix element which depends on the transverse momentum $\mathbf{k}_{2T}^2$, ϕ_2 and ϕ_c are the azimuthal angles of the initial virtual gluon and

the produced quark, respectively. The formula for the resolved photon contribution can be obtained by the similar way. But one should keep in mind that convolution in (6) should be made also with the unintegrated gluon distribution $\mathcal{A}_\gamma(x, \mathbf{k}_T^2, \mu^2)$ in a photon. The final expression for the differential cross section has the form

$$\frac{d\sigma^{(\mathrm{res})}(\gamma p \to c\bar{c} + X)}{dy_c\, d\mathbf{p}_{cT}^2} = \int \frac{|\bar{\mathcal{M}}|^2(g^* g^* \to c\bar{c})}{16\pi (x_1 x_2 s)^2} \times$$
$$\times \mathcal{A}_\gamma(x_1, \mathbf{k}_{1T}^2, \mu^2) \mathcal{A}(x_2, \mathbf{k}_{2T}^2, \mu^2) d\mathbf{k}_{1T}^2 d\mathbf{k}_{2T}^2 dy_{\bar{c}} \frac{d\phi_1}{2\pi} \frac{d\phi_2}{2\pi} \frac{d\phi_c}{2\pi}, \tag{8}$$

where ϕ_1 is the azimuthal angle of the initial virtual gluon having fraction x_1 of a initial photon longitudinal momentum. It is important that the squared off-shell matrix element $|\bar{\mathcal{M}}|^2(g^* g^* \to c\bar{c})$ depends on the both transverse momenta $\mathbf{k}_{1T}^2$ and $\mathbf{k}_{2T}^2$. The analytic expressions for the $|\bar{\mathcal{M}}|^2(\gamma g^* \to c\bar{c})$ and $|\bar{\mathcal{M}}|^2(g^* g^* \to c\bar{c})$ have been evaluated in our previous papers [12, 26]. Note that if we average (7) and (8) over $\mathbf{k}_{1T}$ and $\mathbf{k}_{2T}$ and take the limit $\mathbf{k}_{1T}^2 \to 0$ and $\mathbf{k}_{2T}^2 \to 0$, then we obtain well-known formulas corresponding to the leading-order (LO) QCD calculations.

The recent experimental data [5, 6] taken by the H1 and ZEUS collaborations refer to the $D^{*\pm}$ photoproduction in ep collisions, where the electron is scattered at small angle and the mediating photon is almost real ($Q^2 \sim 0$). Therefore the γp cross sections (7) and (8) need to be weighted with the photon flux in the electron:

$$d\sigma(ep \to c\bar{c} + X) = \int f_{\gamma/e}(y) dy\, d\sigma(\gamma p \to c\bar{c} + X), \tag{9}$$

where y is a fraction of the initial electron energy taken by the photon in the laboratory frame, and we use the Weizacker-Williams approximation for the bremsstrahlung photon distribution from an electron:

$$f_{\gamma/e}(y) = \frac{\alpha_{em}}{2\pi} \left(\frac{1 + (1-y)^2}{y} \ln \frac{Q^2_{\max}}{Q^2_{\min}} + 2m_e^2 y \left(\frac{1}{Q^2_{\max}} - \frac{1}{Q^2_{\min}} \right) \right). \tag{10}$$

Here α_{em} is Sommerfeld's fine structure constant, m_e is the electron mass, $Q^2_{\min} = m_e^2 y^2/(1-y)^2$ and $Q^2_{\max} \sim 1\,\mathrm{GeV}^2$, which is a typical value for the recent photoproduction measurements at HERA.

The multidimensional integration in (7), (8) and (9) has been performed by means of the Monte Carlo technique, using the routine VEGAS [30]. The full C++ code is available from the authors on request[1]. This code is practically identical to that used in [11, 12], with exception that now we apply it to calculate inclusive and jet(s) associated charm production in another kinematical region.

3 Numerical results

We now are in a position to present our numerical results. First we describe our theoretical input and the kinematical conditions. As it was mentioned above, the recent experimental data [5, 6] on the charm photoproduction at HERA come from both H1 and

[1] lipatov@theory.sinp.msu.ru

ZEUS collaboration. The ZEUS measurements [5] are performed in the following kinematical region: $130 < W < 280$ GeV, $Q^2 < 1$ GeV^2, $|\eta^{\rm jet}| < 2.4$, $E_T^{\rm jet} > 6$ GeV, $p_T > 3$ GeV and $-1.5 < \eta < 1.5$. These data have been taken at a proton energy of 920 GeV and an electron energy of 27.5 GeV, which corresponds to a ep center-of-mass (c.m.) energy of $\sqrt{s} = 318$ GeV. Here and in the following all kinematic quantities are given in the laboratory frame where positive OZ axis direction is given by the proton beam. The more recent H1 data [6] refer to the kinematical region defined by $171 < W < 256$ GeV, $Q^2 < 10^{-2}$ GeV^2, $|\eta^{\rm jet}| < 1.5$, $E_T^{\rm jet} > 3$ GeV, $p_T > 2$ GeV and $-1.5 < \eta < 1.5$.

3.1 Theoretical uncertainties

There are several parameters which determined the overall normalization factor of the cross sections (7) and (8): the charm mass m_c, the factorization and normalisation scales μ_F and μ_R and the unintegrated gluon distributions in a proton $\mathcal{A}(x, \mathbf{k}_T^2, \mu^2)$ and in a photon $\mathcal{A}_\gamma(x, \mathbf{k}_T^2, \mu^2)$.

Concerning the unintegrated gluon densities in a proton, we have tried three different sets of the unintegrated gluon densities in a proton, namely J2003 (set 1) [27], KMS [28] and KMR [29]. All these distributions are widely discussed in the literature (see, for example, review [31–33] for more information). Here we only shortly discuss their characteristic properties. First, the J2003 (set 1) gluon density has been obtained [27] from the numerical solution of the full CCFM equation. The input parameters were fitted to describe the proton structure function $F_2(x, Q^2)$. Note that this density contain only singular terms in the CCFM splitting function $P_{gg}(z)$. The J2003 (set 1) distribution has been applied in the analysis of the forward jet production at HERA and charm and bottom production at Tevatron [27] (in the framework of Monte-Carlo generator CASCADE [25]) and has been also used in our calculations [11, 12, 26].

Another set (the KMS) [28] was obtained from a unified BFKL-DGLAP description of early $F_2(x, Q^2)$ data and includes the so-called consistency constraint [34]. The consistency constraint introduces a large correction to the LO BFKL equation. It was argued [34] that about 70% of the full NLO corrections to the BFKL exponent Δ are effectively included in this constraint. The KMS gluon density is successful in description of the beauty hadroproduction at Tevatron [15] and photoproduction at HERA [12].

The last, third unintegrated gluon distribution $\mathcal{A}(x, \mathbf{k}_T^2, \mu^2)$ used here (the so-called KMR distribution) is the one which was originally proposed in [29]. The KMR approach is the formalism to construct unintegrated gluon distribution from the known conventional parton (quark and gluon) densities. It accounts for the angular-ordering (which comes from the coherence effects in gluon emission) as well as the main part of the collinear higher-order QCD corrections. The key observation here is that the μ dependence of the unintegrated parton distribution enters at the last step of the evolution, and therefore single scale evolution equations (DGLAP or unified BFKL-DGLAP) can be used up to this step. Also it was shown [29] that the unintegrated distributions obtained via unified BFKL-DGLAP evolution are rather similar to those based on the pure DGLAP equations. It is because the condition of the angular ordering constraint is more important [29] than including the BFKL effects. Based on this point, in the present paper we use much more simpler DGLAP equation up to the last evolution step in the case of application of the KMR procedure. In the numerical

calculations we have used the standard GRV (LO) parametrizations [35] of the collinear quark and gluon densities. Note that the KMR unintegrated parton distributions in a proton were used, in particular, to describe the prompt photon photoproduction at HERA [13, 36] and prompt photon hadroproduction Tevatron [14, 37].

In the case of a real photon, we have tested two different sets of the unintegrated gluon densities $\mathcal{A}_\gamma(x, \mathbf{k}_T^2, \mu^2)$. First of them was obtained [38] from the numerical solution of the full CCFM equation (which has been also formulated for the photon). Here we will use this gluon density together with the J2003 (set 1) distribution when calculating the resolved photon contribution (8). Also in order to obtain the unintegrated gluon density in a photon we will apply the KMR method [29] to the standard LO GRV parton distributions [35]. In the numerical calculations we will use it together with the KMR distributions in a proton. Note that both gluon densities $\mathcal{A}_\gamma(x, \mathbf{k}_T^2, \mu^2)$ discussed here have been already applied in the analysis of the charm and beauty quark [26, 39] and J/ψ meson production [26] in $\gamma\gamma$ collisions at LEP2.

We would like to point out that at present there is no the unintegrated gluon distribution corresponding to the unified BFKL-DGLAP evolution in a photon. Therefore the resolved photon contribution (8) is not taken into account in the case of KMS gluon distribution.

Significant theoretical uncertainties in our results are connected with the choice of the factorization and renormalization scales. The first of them is related to the evolution of the gluon distributions, the other is responsible for the strong coupling constant $\alpha_s(\mu_R^2)$. As it often done for charm production, we choose the renormalization and factorization scales to be equal: $\mu_R = \mu_F = \mu = \xi\sqrt{m_c^2 + \langle \mathbf{p}_T^2 \rangle}$, where $\langle \mathbf{p}_T^2 \rangle$ is set to the average $\mathbf{p}_T^2$ of the charmed quark and antiquark. In order to investigate the scale dependence of our results we will vary the scale parameter ξ between 1/2 and 2 about the default value $\xi = 1$. Note that we use special choice $\mu^2 = \mathbf{k}_T^2$ in the case of KMS gluon, as it was originally proposed in [27]. The fragmentation $c \to D^*$ is described by Peterson fragmentation function [40] with $\epsilon_c = 0.035$ [41]. The branching ratio $f(c \to D^*)$ was set to the value measured by the OPAL collaboration: $f(c \to D^*) = 0.235$ [42]. For completeness, we take the charmed quark mass $m_c = 1.4$ GeV and use LO formula for the coupling constant $\alpha_s(\mu^2)$ with $n_f = 4$ active quark flavours at $\Lambda_{\rm QCD} = 200$ MeV, such that $\alpha_s(M_Z^2) = 0.1232$.

3.2 Inclusive $D^{*\pm}$ production

The results of our calculations are shown in Figs. 1 — 4 in comparison to the recent H1 experimental data [6]. Instead of presenting our theoretical predictions as continuous lines, we adopt here the binning pattern encoded in the experimental data. The solid, dashed and dash-dotted histograms correspond to the results obtained with the J2003 (set 1), KMR and KMS unintegrated gluon densities, respectively. We observe a reasonable good agreement between our predictions and the H1 experimental data [6] in most of the bins. However, there are some insignificant discrepancies. So, the calculated transverse momentum distribution falls less steeply at large p_T than it is visible in the data. The similar effect was pointed out also in [6] where the massive NLO pQCD approach [18] (FMNR program [43]) and the Monte-Carlo generator CASCADE [35] have been used. Concerning the dependence of our predictions on the evolution scheme, we have found that the $D^{*\pm}$ transverse momentum distribution is only little sensitive to the choice of unintegrated gluon density: very similar

predictions are obtained by all parametrizations (see Fig. 1). This is in agreement with results of the previous investigations [23]. The same situation is observed in W distribution where all gluon densities under consideration predict a very similar shapes. In contrast, the calculated pseudo-rapidity and z distributions strongly depend on the unintegrated gluon density used. Note that pseudo-rapidity distribution additionally has been measured [6] in the three bins of p_T (see Fig. 2). In all these kinematical regions KMR gluon tends to overestimate the data in the rear direction and KMS tends to underestimate the data in the forward one. This is, in particular, due to the fact that gluon-gluon fusion (resolved photon contribution) is not taken into account in the case of KMS gluon in our calculations. At the same time the pseudo-rapidity distributions obtained with the J2003 (set 1) and KMR unintegrated gluon densities (where gluon-gluon fusion contribution is included everywhere) agree well with the H1 data [6] in the forward pseudo-rapidity region. This is in agreement with the general expectations that resolved photon contributions are important at $\eta > 0$.

We would like to point out also that gluon-gluon fusion contributes significantly in the low z region. In order to illustrate this effect we have separately shown the contributions from the photon-gluon (dashed histogram) and gluon-gluon fusion (dash-dotted histogram) mechanisms within the kinematic range of the H1 measurement [6] (see Fig. 3). The solid histogram represents the sum of both these contributions. We have used here the KMR unintegrated gluon density. It is clear that gluon-gluon fusion mechanism is important at low z and should be taken into account in description of the experimental data.

Next, the total inclusive $D^{*\pm}$ photoproduction cross section $\sigma(ep \to e' D^{*\pm} + X)$ has been measured [6] and it was found to be equal to 6.45 ± 0.46 (stat.) ± 0.69 (sys.) nb. The results of our calculations supplemented with the different unintegrated gluon densities are collected in Table 1. The theoretical uncertainties (which are given for the J2003 (set 1) and KMR distributions) are connected with variation on the scale μ^2 as it was described above. The predictions of CASCADE, PYTHIA as well as NLO pQCD calculations (GMVFNS approach and FMNR program) are shown for comparison. The central values from massive NLO pQCD calculations (FMNR program) and from CASCADE are slightly lower than the measured result, whereas those of PYTHIA [44] and GMVFNS [20] are higher. One can see that our predictions are rather close to ones from the CASCADE and FMNR programs and reasonably agree with the H1 data within the theoretical and experimental uncertainties. Also we estimate the individual contributions from the photon-gluon and gluon-gluon fusion to the total cross section in the k_T-factorization approach. We have found it to be about 80% and 20%, respectively. Additionally we investigate the scale dependence of our predictions (see Fig. 4). In these plots the solid histograms were obtained by fixing both the factorization and normalization scales at the default value μ^2, whereas upper and lower dashed histograms correspond to the scale variation as it was described above. Here we have used the KMR unintegrated gluon density. One can see that scale variation changes the normalization of predicted cross section by $20 - 30\%$ approximately. Note that we have not varied the charmed quark mass and used the default value of m_c in all calculations.

3.3 Associated $D^{*\pm}$ and single jet production

Now we demonstrate how k_T-factorization approach can be used to calculate the semi-inclusive charm photoproduction rates. The basic photon-gluon or gluon-gluon fusion sub-

Source	$\sigma(ep \to e' D^{*\pm} + X)$ [nb]
H1 measurement [6]	6.45 ± 0.46 (stat.) ± 0.69 (sys.)
CASCADE [25]	$5.38^{+0.54}_{-0.62}$
PYTHIA [45]	8.9
FMNR [44]	$5.9^{+2.8}_{-1.3}$
GMVFNS [20]	$8.2^{+5.3}_{-4.0}$
J2003 (set 1)	$4.92^{+1.15}_{-0.72}$
KMR	$6.57^{+1.80}_{-1.48}$
KMS	5.10

Table 1: The total cross section of the inclusive $D^{*\pm}$ photoproduction in electron-proton collisions at $Q^2 < 10^{-2}$ GeV^2, $0.29 < y < 0.65$, $p_T > 2$ GeV and $-1.5 < \eta < 1.5$.

processes under consideration give rise to two high-energy charmed quarks, which can further evolve into hadron jets. In our calculations the produced quarks (with their known kinematical parameters) were taken to play the role of the final jets. These two quarks are accompanied by a number of gluons radiated in the course of the gluon evolution. As it has been noted in [22], on the average the gluon transverse momentum decreases from the hard interaction block towards the proton. As an approximation, we assume that the gluon emitted in the last evolution step and having the four-momenta k' compensates the whole transverse momentum of the gluon participating in the hard subprocess, i.e. $\mathbf{k}'_T = -\mathbf{k}_T$. All the other emitted gluons are collected together in the proton remnant, which is assumed to carry only a negligible transverse momentum compared to $\mathbf{k}'_T$. This gluon gives rise to a final hadron jet with $E_T^{\rm jet} = |\mathbf{k}'_T|$ in addition to the jet produced in the hard subprocess. From these three hadron jets we choose the one jet (or two jets) carrying the largest transverse energy, and then compute the charm and associated jet(s) production rates.

In the recent analysis [5, 6] performed by of the H1 and ZEUS collaborations jets are divided into two categories: jets of the first category are associated with the $D^{*\pm}$ meson (D^*-tagged jet), while jets of the second category are not matched to a $D^{*\pm}$ meson (D^*-untagged jet). The inclusive, D^*-tagged and untagged jet cross sections have been measured [5] by the ZEUS collaboration whereas H1 data refer to the D^* and untagged jet cross sections only [6]. Note that formulation of the ZMVFNS do not provide the possibility to simultaneously determine kinematic variables related to the $D^{*\pm}$ meson and the jet that includes it, so that a comparison to the massless NLO pQCD calculations is only available for the untagged jet cross sections [45]. In the following we will systematically compare the predictions from the k_T-factorization approach to all published data on associated charm and single jet production at HERA.

3.3.1 D^*-tagged jets: $p_T^{\rm jet}$ and $\eta^{\rm jet}$ distributions

The results of our calculations are shown in Fig. 5 in comparison to the ZEUS experimental data [5]. Notations of all histograms here are the same as in Fig. 1. The pseudo-rapidity $\eta^{\rm jet}$ distribution additionally has been measured in the three bins of $E_T^{\rm jet}$. One can see that shape of the data is well described by our predictions, although the normalisation is un-

derestimated (by a factor of 1.5). However, this discrepancy is not dramatic, because some reasonable variations in charm mass m_c, energy scale μ^2 or $\Lambda_{\rm QCD}$ parameter (not shown in Figs.) can partially cover the visible disagreement. It is interesting that difference between the theoretical predictions calculated with different unintegrated gluon densities in a proton are somewhat less pronounced in comparison to the inclusive $D^{*\pm}$ production case. The KMS gluon tends to predict a larger cross sections than ones obtained with other gluon densities under consideration. This fact is in contrast with the results presented in the previous section where KMR gluon dominates. The possible explanation is connected with the difference in the kinematical region (in which our predictions as well as experimental data were presented). We would like to point out also that our central predictions are very similar to the massive NLO pQCD results [18]. It was claimed [5] that normalisation of the ZEUS data for all distributions is reasonable described by the upper limit of these NLO pQCD calculations.

3.3.2 D^*-untagged jets: $x_\gamma^{\rm obs}(D^*)$ distribution

Now we turn to the $D^{*\pm}$ and untagged jet production. First we discuss the very interesting subject of study which is connected with the individual contributions from the direct and resolved photon mechanisms. As it was already mentioned above, the $x_\gamma^{\rm obs}(D^*)$ variable (which corresponds at leading order to the fraction of the exchanged photon momentum in the hard scattering process) provides a tool to investigate the relative importance of these different contributions. In LO collinear approximation, direct photon events at parton level have $x_\gamma^{\rm obs}(D^*) \sim 1$, while the resolved photon events populate the low values of $x_\gamma^{\rm obs}(D^*)$. The same situation is observed in a NLO calculations, because in the three parton final state any of these partons are allowed to take any kinematically accessible value. In the k_T-factorization formalism the hardest transverse momentum parton emission can be anywhere in the evolution chain, and does not need to be closest to the photon as required by the strong μ^2 ordering in DGLAP. Thus, if hardest jet originates from the $c\bar{c}$ pair, then $x_\gamma^{\rm obs}(D^*)$ is close to unity, but if a gluon from the initial cascade form the hardest transverse momentum jet, then $x_\gamma^{\rm obs}(D^*) < 1$. This statement is clearly demonstrated in Fig. 6 where separately shown the contributions from the photon-gluon (dashed histogram) and gluon-gluon fusion (dash-dotted histogram) subprocesses within the kinematic range of the ZEUS measurement [5]. The solid histogram represents the sum of both these contributions. We have used here the KMR unintegrated gluon density for illustration. In agreement with the expectation for direct photon processes, the peak at high values of the $x_\gamma^{\rm obs}(D^*)$ is observed. However, one can see that off-shell photon-gluon fusion results also in substantial tail at small values of $x_\gamma^{\rm obs}(D^*)$. The existence of this plateau in the collinear approximation of QCD usually is attributted to the charmed quark excitation from resolved photon. In the k_T-factorization approach such plateau indicates the fact that the gluon radiated from evolution cascade appears to be harder than charmed quarks (produced in hard parton interaction) in a significant fraction of events [11, 22]. Therefore we can conclude that the k_T-factorization formalism effectively imitates the charm component of the photon [11, 22]. However, the predicted tail at small $x_\gamma^{\rm obs}(D^*)$ values is strongly depends on the unintegrated gluon distributions used, as it was demonstrated in [11]. Note that the gluon-gluon fusion events (with a gluon coming from the photon) are distributed over the whole $x_\gamma^{\rm obs}(D^*)$ range.

It is clear that these events play role at small values of $x_\gamma^{\rm obs}(D^*)$ only and that now the total contribution to the cross section from the gluon inside the resolved photon is too small to be useful[2]. This fact is in contrast with the inclusive $D^{*\pm}$ production case and coincide with the results [45] obtained in the massless NLO QCD approximation.

In Fig. 7 we confront the calculated $x_\gamma^{\rm obs}(D^*)$ distribution with the ZEUS data [5]. One can see that our results corresponding to different gluon densities do not agree well with the ZEUS data. If this disagreement is true, then the possible explanation of this fact is the following. The calculated cross sections at low $x_\gamma^{\rm obs}(D^*)$ are defined by the average value of the gluon transverse momenta $\langle k_T \rangle$ which is generated in the course of the non-colliner evolution. It is due to the fact that events when the gluon jet has the largest p_T among the three hadron jets contribute only in this kinematical region. So, this average gluon $\langle k_T \rangle$ which generated by the all three versions of the unintegrated gluon distributions under consideration possible could be too small to describe the ZEUS data. The similar situation was observed in [11] where the $D^{*\pm}$ and dijet associated photoproduction has been considered. However, the k_T-factorization approach well describes the experimental data with the cut on the dijet invariant mass $M > 18$ GeV [11]. It demonstrates that this cut is essential for applicability of the description of resolved photon contributions by non-collinear evolution in a proton only. Therefore we can conclude that further theoretical and experimental investigations are necessary in order to understand and adequatively describe the ZEUS experimental data in the low $x_\gamma^{\rm obs}(D^*)$ region.

3.3.3 D^*-untagged jets: p_T, η, $p_T^{\rm jet}$ and $\eta^{\rm jet}$ distributions

In Figs. 8 — 10 we confront the differential cross section of $ep \to D^{*\pm} + {\rm jet} + X$ in photoproduction as measured [5, 6] by H1 and ZEUS collaborations with our predictions. One can see in Fig. 8 that the differential cross section as a function of η and $p_T^{\rm jet}$ measured by the H1 collaboration is well described (both in shape and in magnitude) by our calculations. Also the predicted cross section as a function of $\eta - \eta^{\rm jet}$ (see Fig. 10) are in a good agreement with the experimental data. Note that there is some difference in shape of the $\eta^{\rm jet}$ distribution between the data and our calculations. Similar to inclusive $D^{*\pm}$ production case, all unintegrated gluon densities under consideration slightly overestimate the $d\sigma/dp_T$ distribution at large p_T (see Fig. 8). But in general the H1 data on the total and differential cross sections are reasonable well reproduced by our calculations. In Table 2 the estimations of total cross section obtained from our calculations as well as from CASCADE, PYTHIA, massive and massless NLO pQCD evaluations are listed and compared with the H1 data [6]. The theoretical uncertainties (which are given for the J2003 (set 1) and KMR distributions) are connected with variation on the scale μ^2, as it was made earlier in the inclusive $D^{*\pm}$ production case.

Concerning the ZEUS measurement, the situation is not clear, as it seen from Fig. 9. One can see that transverse energy distribution is underestimated in all $E_T^{\rm jet}$ bins. The difference in normalisation between our predictions and the ZEUS data is about 1.5 or

[2]This is one of reasons why the values of our cross sections (see Table 1 and 2) obtained with the J2003 (set 1) unintegrated gluon distribution are not more the CASCADE predictions. The main reasons of this distinction are the different factorization scales in our calculations and the CASCADE ones and also the account for the initial and final showers in the MC generator CASCADE [6].

Source	$\sigma(ep \to e' D^{*\pm} + \text{jet} + X)$ [nb]
H1 measurement [6]	3.01 ± 0.29 (stat.) ± 0.33 (sys.)
CASCADE [25]	$3.08^{+0.22}_{-0.28}$
PYTHIA [45]	3.8
FMNR [44]	$2.65^{+0.78}_{-0.42}$
ZMVFNS [46]	$3.05^{+0.62}_{-0.47}$
J2003 (set 1)	$2.47^{+0.60}_{-0.39}$
KMR	$3.61^{+0.84}_{-0.68}$
KMS	3.11

Table 2: The total cross section of the associated $D^{*\pm}$ and single jet photoproduction in electron-proton collisions at $Q^2 < 0.01$ GeV^2, $0.29 < y < 0.65$, $p_T > 2$ GeV, $-1.5 < \eta < 1.5$, $p_T^{\text{jet}} > 3$ GeV and $-1.5 < \eta^{\text{jet}} < 1.5$.

even 2. This fact is in clear contrast with comparison of our theoretical results with the H1 measurements. Also the shape of measured η^{jet} distributions is very different from the calculated one. Particularly, the ZEUS data are overshoot our theoretical estimations in the forward direction. But a good agreement is achieved in the rear pseudo-rapidity region (namely, at $\eta^{\text{jet}} < 0.5$). The similar situation is obtained [5] in the framework of both massive and massless NLO pQCD approaches [43, 45].

Now we turn to some qualitative comparison between the predictions of k_T-factorization approach and the ones obtained in the framework of collinear NLO pQCD approximation. It is well known that in the case of inclusive single hadron photoproduction the direct and resolved photon contributions are accumulated in the backward and forward directions, respectively. Using the ZMVFNS scheme, it was shown [45] that the pseudo-rapidity η^{jet} of D^*-untagged jet (but not pseudo-rapidity η of the $D^{*\pm}$ meson) can serve as a discriminator between these two contributions. It is because the shapes of direct and resolved photon mechanism are very different to each other. In Fig. 11 we split our central predictions for $d\sigma/d\eta^{\text{jet}}$ distribution calculated in the ZEUS kinematical region into their direct and resolved photon components using the $x_\gamma^{\text{obs}}(D^*)$ variable and show the results as the solid and dashed histograms, respectively. We have used the KMR unintegrated gluon densities in a proton and in a photon. Similar to massless NLO pQCD [45], we obtain a strong different behaviour of calculated cross sections at $x_\gamma^{\text{obs}}(D^*) > 0.75$ and $x_\gamma^{\text{obs}}(D^*) < 0.75$. Moreover, we reproduce well the direct contribution both in normalization and shape (see also Fig. 8 from Ref. [45]). But predicted resolved photon component lie below NLO pQCD one by a factor of about 2, although agree with NLO pQCD results in a shape. The observed difference in normalisation is strongly depends, of course, on the unintegrated gluon distribution used. In particular, difference between our calculations and results presented in [45] indicates again that average gluon $\langle k_T \rangle$ is too small and that further theoretical investigations of non-collinear gluon evolution are needed. However, at qualitative level, the k_T-factorization formalism in a simplest way reproduces well the basic properties of the standard fixed-order calculations for process under consideration.

3.3.4 D^*-untagged jets: $\cos\theta^*$ variable

Next we turn to the different angular correlations in the charm production at HERA. First we discuss the $\cos\theta^*$ variable. As it was already mentioned above, studying of distribution on $\cos\theta^*$ also give us the possibility to learn about the size of the contribution from different production mechanisms. It is because this quantity is sensitive to the spin of the propagator in the hard subprocess [5]. In direct photon processes $\gamma g \to c\bar{c}$ the propagator in the LO QCD diagrams is a quark, and the differential cross section rises slowly towards high $|\cos\theta^*|$ values, namely proportional to $(1 - |\cos\theta^*|)^{-1}$. In resolved processes, the gluon propagator is allowed at LO and dominates over the quark propagator due to the stronger gluon-gluon coupling compared to the quark-gluon coupling. If most of the resolved photon events are produced as a result of charm from the photon, a gluon-exchange contribution in $cg \to cg$ subprocess should dominate. This results in a steep rise of the cross section towards high $|\cos\theta^*|$ values: $d\sigma/d\cos\theta^* \sim (1 - |\cos\theta^*|)^{-2}$. A recent ZEUS analysis [5] on dijet angular distributions in the $D^{*\pm}$ photoproduction has shown that the measured cross section from resolved-enriched events (i.e. events with $x_\gamma^{\rm obs}(D^*) < 0.75$) exhibits a distinct asymmetry with a strong rise towards $\cos\theta^* = -1$. This behaviour suggest that events with $x_\gamma^{\rm obs}(D^*) < 0.75$ are dominantly produced by charmed quarks coming from the photon side. On the other hand, the $\cos\theta^*$ distribution for direct-enriched events (where $x_\gamma^{\rm obs}(D^*) > 0.75$) is almost symmetric. In the k_T-factorization approach the $\cos\theta^*$ distribution is determined only by the photon-gluon fusion off-shell matrix element which cover both scattering process (since there is no restriction on the transverse momenta along the evolution cascade, as it was already discussed above). In order to study this quantity in a detail, in Fig. 12 we show the differential cross section as a function of $\cos\theta^*$ for the direct-enriched (solid histogram) and resolved-enriched (dashed histogram) samples separately within the kinematic range of the ZEUS experiment. We have used here the KMR unintegrated gluon density for illustration. One can see that resolved photon-like events exhibit a strong rise towards $\cos\theta^* = -1$, i.e. in photon direction, consistent with a dominant contribution from gluon exchange. In our theoretical calculations, the peak at $\cos\theta^* = -1$ at low $x_\gamma^{\rm obs}(D^*)$ clearly illustrates again that the k_T-factorization approach effectively reproduces the charm excitation processes using only the photon-gluon fusion off-mass shell matrix elements. However, we should point out that the absolute normalization of this peak differs from the one calculated [45] in the massless NLO pQCD approximation (by a factor of about 2). This fact is in a full agreement with the results presented in the previous section (in Fig. 11) and indicates again that resolved photon contribution is underestimated by our calculations (compared to the NLO pQCD ones). Unfortunately, at present there is no experimental data on $\cos\theta^*$ distribution in the associated $D^{*\pm}$ and single jet photoproduction. Therefore additional experimental efforts in this field possible can give us the possibility to better constraint the unintegrated gluon density in a proton.

3.3.5 D^*-untagged jets: azimuthal correlations

Further understanding of the process dynamics and in particular of the high-order correction effects may be obtained from the transverse correlation between the produced $D^{*\pm}$ meson and the jet. The H1 collaboration has measured [6] the distribution on the $\Delta\phi$ angle, which is the difference in azimuth between the $D^{*\pm}$ meson and the jet. In the naive leading

order approximation, the distribution over $\Delta\phi$ must be simply a delta function $\delta(\Delta\phi - \pi)$, since the produced $D^{*\pm}$ meson and the jet are back-to-back in the transverse plane. Taking into account the non-vanishing initial parton transverse momenta $\mathbf{k}_{1T}$ and $\mathbf{k}_{2T}$ leads to the violation of this back-to-back kinematics in the k_T-factorization approach [15].

The calculated $\Delta\phi$ distributions are shown in Fig. 13 in comparison to the H1 data. Additionally, in Figs. 14 and 15 we plot our predictions separately for the regions $x_\gamma^{\rm obs}(D^*) > 0.75$ and $x_\gamma^{\rm obs}(D^*) < 0.75$, where direct and resolved photon induced processes dominate, respectively. Last results have been calculated for the ZEUS kinematical range, as it was described above. It is clear that k_T-factorization approach predicts a large fraction of events where the $D^{*\pm}$ and the jet are not back-to-back. The measured deviations from the back-to-back topology are reasonable well described by our calculations. Best agreement is achieved using the KMR unintegrated gluon density. There is general behaviour of theoretical results obtained using the unintegrated gluon densities under consideration. All of them overestimate the H1 data at $\Delta\phi \sim 0$ (where gluon $\mathbf{k}_T$ is large) as well as at $\Delta\phi \sim \pi$, i.e. in the back-to-back region. But at moderate $\Delta\phi$ our predictions tends to underestimate the data. One can see that region of low $\Delta\phi$ is very sensitive to the unintegrated gluon distributions: the difference between predictions can be one order of magnitude (see Figs. 14 and 15). The similar results has been obtained in [11, 15]. Therefore we can expect that further theoretical and experimental studying of these correlations will give important information about non-collinear parton evolution dynamics in a proton and in a photon.

4 Conclusions

We have investigated the charm photoproduction in electron-proton collisions at HERA using the k_T-factorization approach of QCD. Our analysis cover the inclusive charm production as well as charm and associated jet production processes. Both photon-gluon (direct) and gluon-gluon fusion (resolved) mechanisms were taken into account. Our investigations were based on the leading-order off-shell matrix elements of the relevant partonic subprocesses. The total and differential cross sections have been calculated and the comparisons to the recent H1 and ZEUS experimental data have been made. In numerical analysis we have used the unintegrated gluon densities which are obtained from the full CCFM, from unified BFKL-DGLAP evolution equations as well as from the Kimber-Martin-Ryskin prescription.

We have shown that the k_T-factorization approach reproduces reasonably well the numerous H1 data on both inclusive charm and associated charm and jet production. At the same time we find that the ZEUS measurements overshoot our theoretical predictions by a factor of about 1.5 or even 2. It means that additional efforts should be done from both the theoretical and experimental sides in order to reduce this disagreement.

We find that our results agree with the standard NLO pQCD ones at qualitative level for process under consideration. It was demonstrated that off-shell matrix elements combined with the non-collinear evolution of gluon densities in a proton effectively simulate the charmed quark excitation processes. We find that resolved photon contributions are underestimated in the framework of k_T-factorization formalism compared to the massless NLO pQCD calculations. Of course, degree of this underestimation strongly depends on the unintegrated gluon density used.

Special attention in our calculations has been drawn to the specific angular correlations between the produced $D^{*\pm}$ meson and jets in final state. In particular, we demostrate the strong sensitivity of the $\Delta\phi$ distribution at low $\Delta\phi$ to the unintegrated gluon densities in a proton and in a photon.

To conclude, we believe that the k_T-factorization formalism holds a possible key to understanding charm production at HERA. However, there are still large uncertainties, and much more work needs to be done.

5 Acknowledgements

We thank H. Jung for possibility to use the CCFM code for inintegrated dluon distributions in our calculations, for careful reading of the manuscript and critical remarks. The authors are very grateful to S.P. Baranov for encouraging interest and very helpful discussions, S. Chekanov and J. Loizides for discussion of the ZEUS data, P.F. Ermolov for the support and DESY Directorate for the support and the hospitality. A.V.L. was supported in part by the grant of President of Russian Federation (MK-9820.2006.2). Also this research was supported by the FASI of Russian Federation (grant NS-8122.2006.2).

References

[1] C. Adloff *et al.* (H1 Collaboration), Nucl. Phys. B **545**, 21 (1999).

[2] J. Breitweg *et al.* (ZEUS Collaboration), Eur. Phys. J. C **6**, 67 (1999).

[3] S. Chekanov *et al.* (ZEUS Collaboration), Phys. Lett. B **565**, 87 (2003).

[4] A. Aktas *et al.* (H1 Collaboration), Phys. Lett. B **621**, 56 (2005).

[5] S. Chekanov *et al.* (ZEUS Collaboration), Nucl. Phys. B **729**, 492 (2005).

[6] A. Aktas *et al.* (H1 Collaboration), DESY 06-110.

[7] S. Catani, M. Ciafoloni and F. Hautmann, Nucl. Phys. B **366**, 135 (1991).

[8] J.C. Collins and R.K. Ellis, Nucl. Phys. B **360**, 3 (1991).

[9] L.V. Gribov, E.M. Levin, and M.G. Ryskin, Phys. Rep. **100**, 1 (1983).

[10] E.M. Levin, M.G. Ryskin, Yu.M. Shabelsky and A.G. Shuvaev, Sov. J. Nucl. Phys. **53**, 657 (1991).

[11] A.V. Lipatov and N.P. Zotov, Eur. Phys. J. C **47**, 643 (2006).

[12] A.V. Lipatov and N.P. Zotov, Phys. Rev. D **73**, 114018 (2006);
A.V. Lipatov and N.P. Zotov, JHEP **0608**, 043 (2006).

[13] A.V. Lipatov and N.P. Zotov, Phys. Rev. D **72**, 054002 (2005).

[14] A.V. Lipatov and N.P. Zotov, DESY 05-157, to be published in J. Phys. G (2007).

[15] S.P. Baranov, N.P. Zotov and A.V. Lipatov, Phys. Atom. Nucl. **67**, 834 (2004).

[16] E.A. Kuraev, L.N. Lipatov, and V.S. Fadin, Sov. Phys. JETP **44**, 443 (1976);
E.A. Kuraev, L.N. Lipatov, and V.S. Fadin, Sov. Phys. JETP **45**, 199 (1977);
I.I. Balitsky and L.N. Lipatov, Sov. J. Nucl. Phys. **28**, 822 (1978).

[17] M. Ciafaloni, Nucl. Phys. B **296**, 49 (1988);
S. Catani, F. Fiorani, and G. Marchesini, Phys. Lett. B **234**, 339 (1990);
S. Catani, F. Fiorani, and G. Marchesini, Nucl. Phys. B **336**, 18 (1990);
G. Marchesini, Nucl. Phys. B **445**, 49 (1995).

[18] V.N. Gribov and L.N. Lipatov, Yad. Fiz. **15**, 781 (1972);
L.N. Lipatov, Sov. J. Nucl. Phys. **20**, 94 (1975);
G. Altarelly and G. Parizi, Nucl. Phys. B **126**, 298 (1977);
Y.L. Dokshitzer, Sov. Phys. JETP **46**, 641 (1977).

[19] S. Frixione, P. Nason and G. Ridolfi, Nucl. Phys. B **454**, 3 (1995).

[20] J. Binnewies, B.A. Kniehl and G. Kramer, Z. Phys. C **76**, 677 (1997);
B.A. Kniehl, G. Kramer and M. Spira, Z. Phys. C **76**, 689 (1997);
J. Binnewies, B.A. Kniehl and G. Kramer, Phys. Rev. D **48**, 014014 (1998).

[21] J.C. Collins, Phys. Rev. D **58**, 094002 (1998);
M.A.G. Aivazis, J.C. Collins, F.I. Olness and W.-K. Tung, Phys. Rev. D **50**, 3102 (1994);
F.I. Olness, R.J. Scalise and W.-K. Tung, Phys. Rev. D **59**, 014506 (1999);
A. Chuvakin, J. Smith and W.L. van Neerven, Phys. Rev. D **61**, 096004 (2000).

[22] S.P. Baranov and N.P. Zotov, Phys. Lett. B **491**, 111 (2000).

[23] S.P. Baranov, H. Jung, L. Jönsson, S. Padhi and N.P. Zotov, Eur. Phys. J. C **24**, 425 (2002).

[24] M. Luszczak and A. Szczurek, Phys. Lett. B **594**, 291 (2004);
Phys. Rev. D **73**, 054028 (2006).

[25] H. Jung, Comput. Phys. Comm. **143**, 100 (2002).

[26] A.V. Lipatov and N.P. Zotov, Eur. Phys. J. C **41**, 163 (2005).

[27] H. Jung, Mod. Phys. Lett. A **19**, 1 (2004).

[28] J. Kwiecinski, A.D. Martin and A. Stasto, Phys. Rev. D **56**, 3991 (1997).

[29] M.A. Kimber, A.D. Martin and M.G. Ryskin, Phys. Rev. D **63**, 114027 (2001);
G. Watt, A.D. Martin and M.G. Ryskin, Eur. Phys. J. C **31**, 73 (2003).

[30] G.P. Lepage, J. Comput. Phys. **27**, 192 (1978).

[31] B. Andersson *et al.* (Small-x Collaboration), Eur. Phys. J. C **25**, 77 (2002).

[32] J. Andersen *et al.* (Small-x Collaboration), Eur. Phys. J. C **35**, 67 (2004).

[33] J. Andersen *et al.* (Small-x Collaboration), Eur. Phys. J. C **48**, 53 (2006).

[34] J. Kwiecinski, A.D. Martin and A. Sutton, Phys. Rev. D **52**, 1445 (1995);
J. Kwiecinski, A.D. Martin and J. Outhwaite, Eur. Phys. J. C **9**, 611 (2001).

[35] M. Glück, E. Reya and A. Vogt, Phys. Rev. D **46**, 1973 (1992);
M. Glück, E. Reya and A. Vogt, Z. Phys. C **67**, 433 (1995).

[36] S. Chekanov *et al.* (ZEUS Collaboration), DESY 06-125.

[37] M.A. Kimber, A.D. Martin and M.G. Ryskin, Eur. Phys. J. C **12**, 655 (2001).

[38] M. Hansson, H. Jung and L. Jönsson, hep-ph/0402019.

[39] L. Motyka and N. Timneanu, Eur. Phys. J. C **27**, 73 (2003).

[40] C. Peterson, D. Schlatter, I. Schmitt, and P. Zerwas, Phys. Rev. D **27**, 105 (1983).

[41] P. Nason and C. Oleari, Nucl. Phys. B **565**, 245 (2000).

[42] K. Ackerstaff *et al.* (OPAL Collaboration), Eur. Phys. J. C **1**, 439 (1997).

[43] S. Frixione, M.L. Mangano, P. Nason and G. Ridolfi, Phys. Lett. B **348**, 633 (1995).

[44] T. Sjöstrand *et al.*, Comput. Phys. Comm. **135**, 238 (2001).

[45] G. Heinrich and B.A. Kniehl, Phys. Rev. D **70**, 094035 (2004).

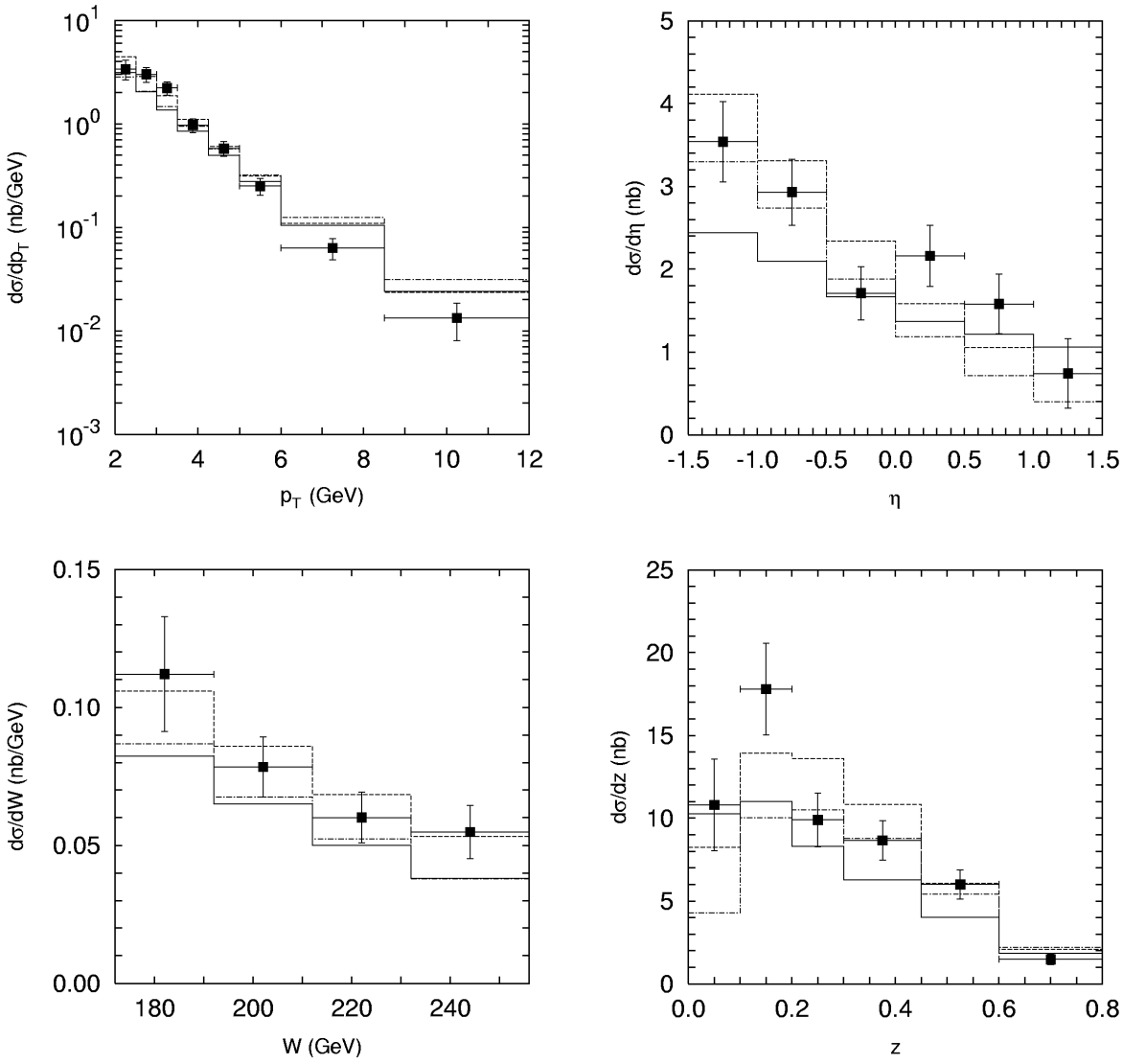

Figure 1: The differential cross sections of the inclusive $D^{*\pm}$ production at HERA calculated in the kinematic range $Q^2 < 0.01$ GeV^2, $0.29 < y < 0.65$, $p_T > 2$ GeV and $-1.5 < \eta < 1.5$. The solid, dashed and dash-dotted histograms correspond to the predictions obtained with the J2003 (set 1), KMR and KMS unintegrated gluon densities, respectively. The experimental data are from H1 [6].

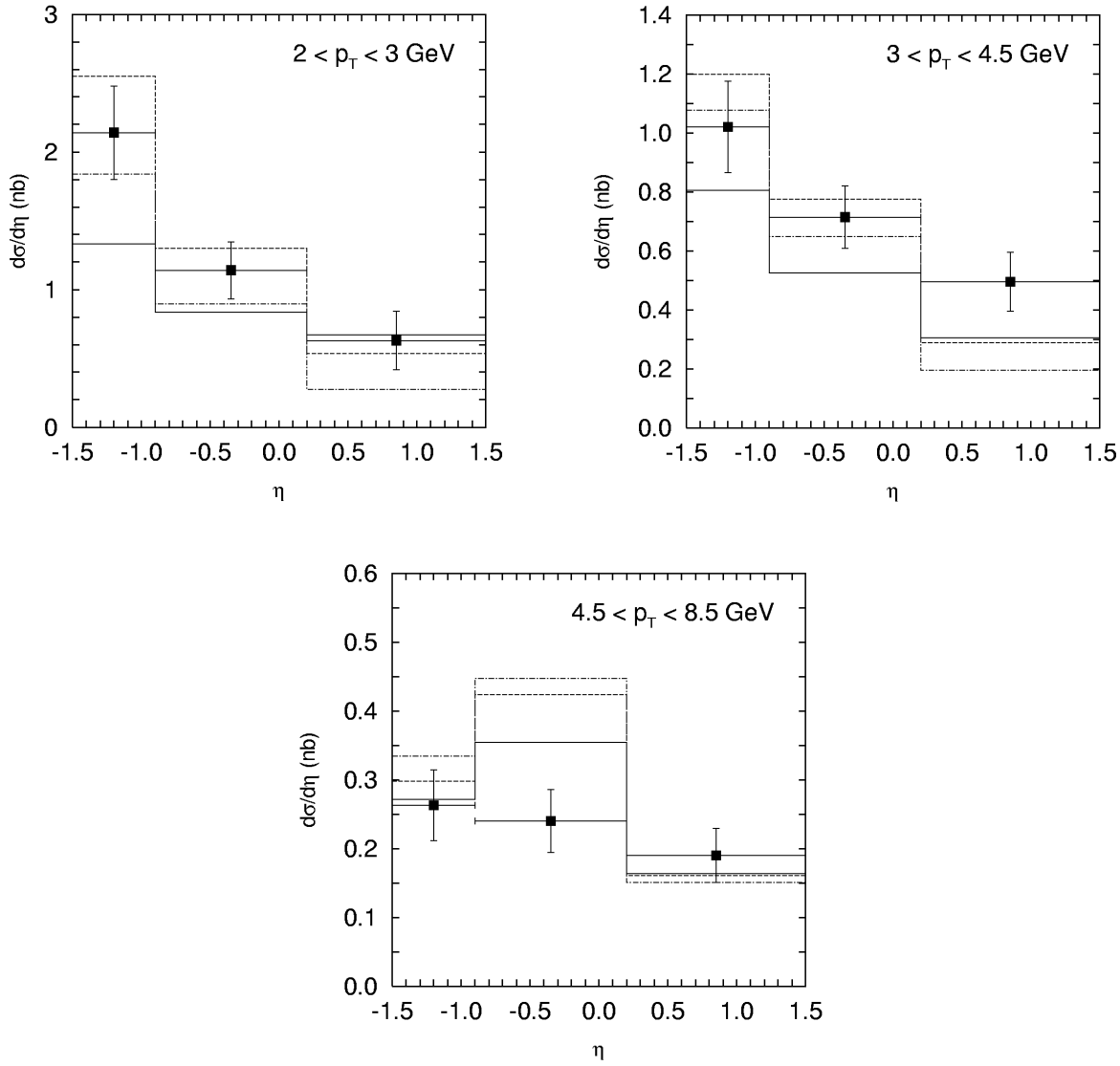

Figure 2: Inclusive $D^{*\pm}$ cross sections as a function of η for three bins of p_T. Notations of all histograms here are the same as in Fig. 1. The experimental data are from H1 [6].

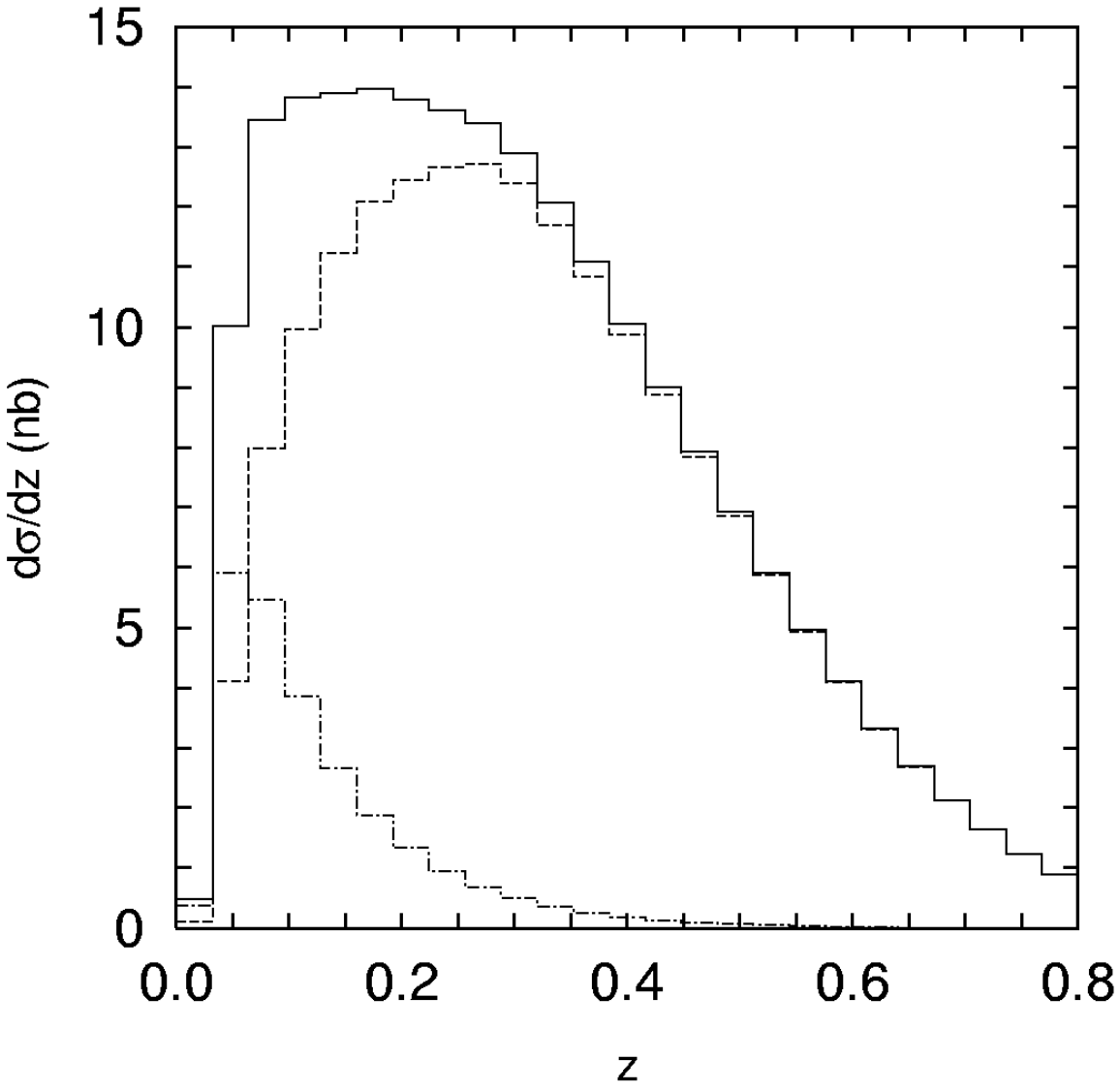

Figure 3: The $d\sigma/dz$ distribution of the inclusive $D^{*\pm}$ production at HERA calculated in the kinematic range $Q^2 < 0.01$ GeV^2, $0.29 < y < 0.65$, $p_T > 2$ GeV and $-1.5 < \eta < 1.5$. Separately shown the contributions from the photon-gluon (dashed histogram) and gluon-gluon (dash-dotted histogram). Solid histogram represents the sum of both these contributions. The KMR unintegrated gluon densities in a proton and in a photon have been used.

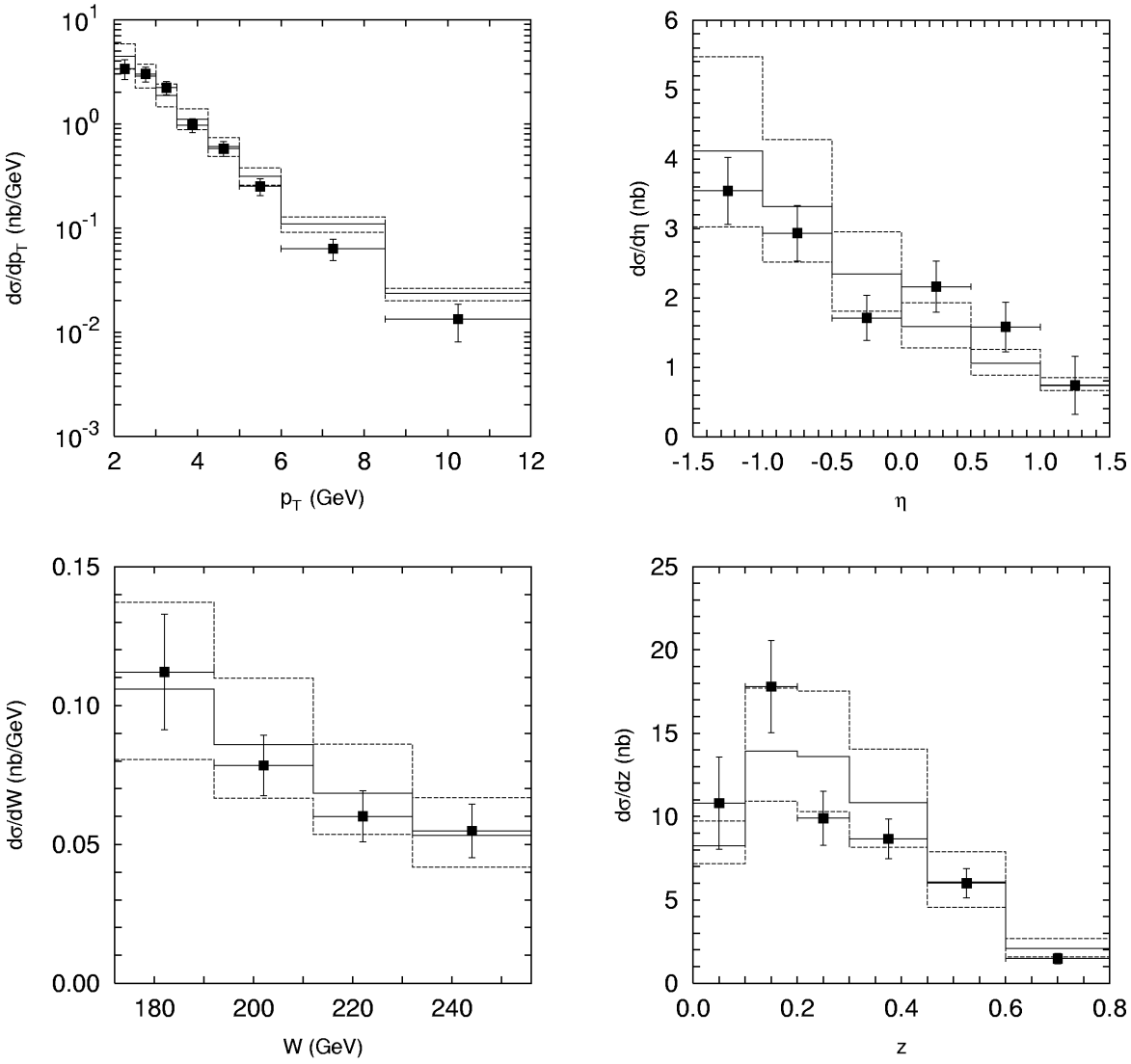

Figure 4: The $d\sigma/dp_T$ distribution of the inclusive $D^{*\pm}$ production at HERA calculated in the kinematic range $Q^2 < 0.01$ GeV^2, $0.29 < y < 0.65$ and $-1.5 < \eta < 1.5$. Solid, upper dashed and lower dashed histograms were obtained with the $\mu^2 = m_T^2$, $\mu^2 = 1/4m_T^2$ and $\mu^2 = 4m_T^2$, respectively. The experimental data are from H1 [6].

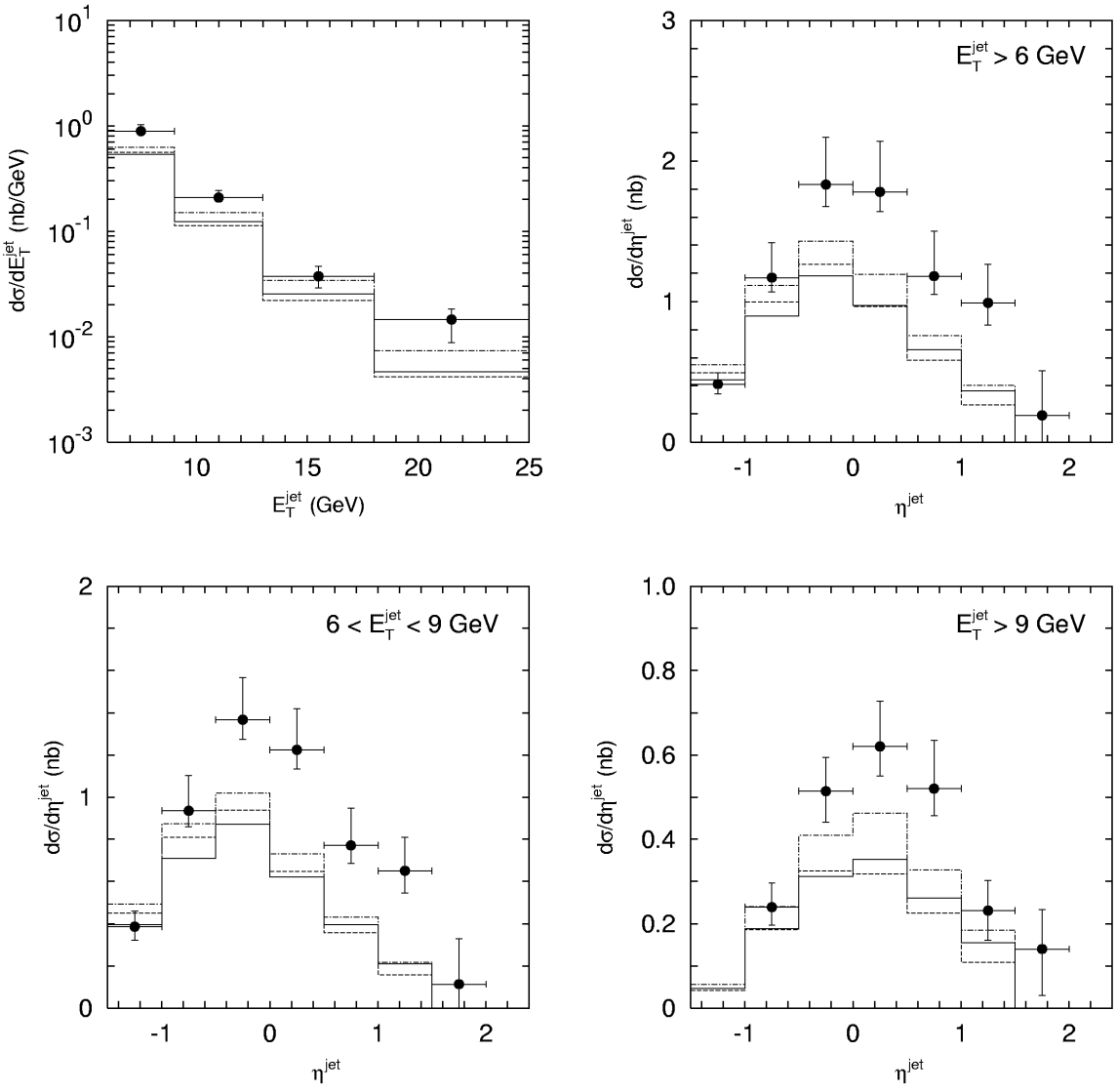

Figure 5: The differential cross sections of the $D^{*\pm}$ and tagged jet production at HERA calculated in the kinematic range $Q^2 < 1$ GeV^2, $130 < W < 280$ GeV, $p_T > 3$ GeV, $|\eta| < 1.5$, $-1.5 < \eta^{\rm jet} < 2.4$ and $E_T^{\rm jet} > 6$ GeV. Notations of all histograms here are the same as in Fig. 1. The experimental data are from ZEUS [5].

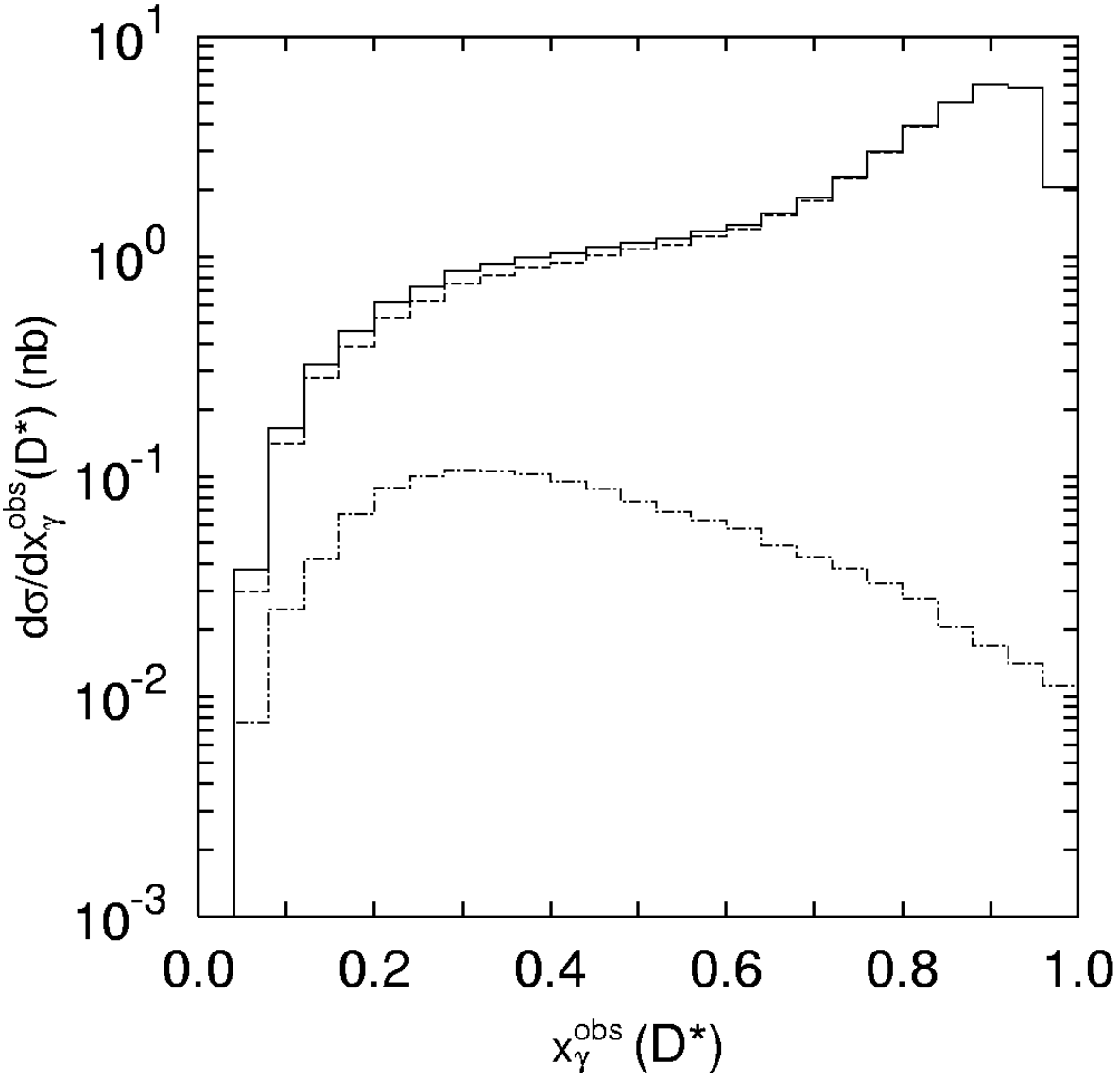

Figure 6: Direct (dashed histogram) and resolved photon (dashed-dotted histogram) components of our central predictions of the differential cross section $d\sigma/dx_\gamma^{\rm obs}(D^*)$ calculated in the kinematic range $Q^2 < 1$ GeV^2, $130 < W < 280$ GeV, $p_T > 3$ GeV, $|\eta| < 1.5$, $-1.5 < \eta^{\rm jet} < 2.4$ and $E_T^{\rm jet} > 6$ GeV. The KMR unintegrated gluon densities in a proton and in a photon have been used.

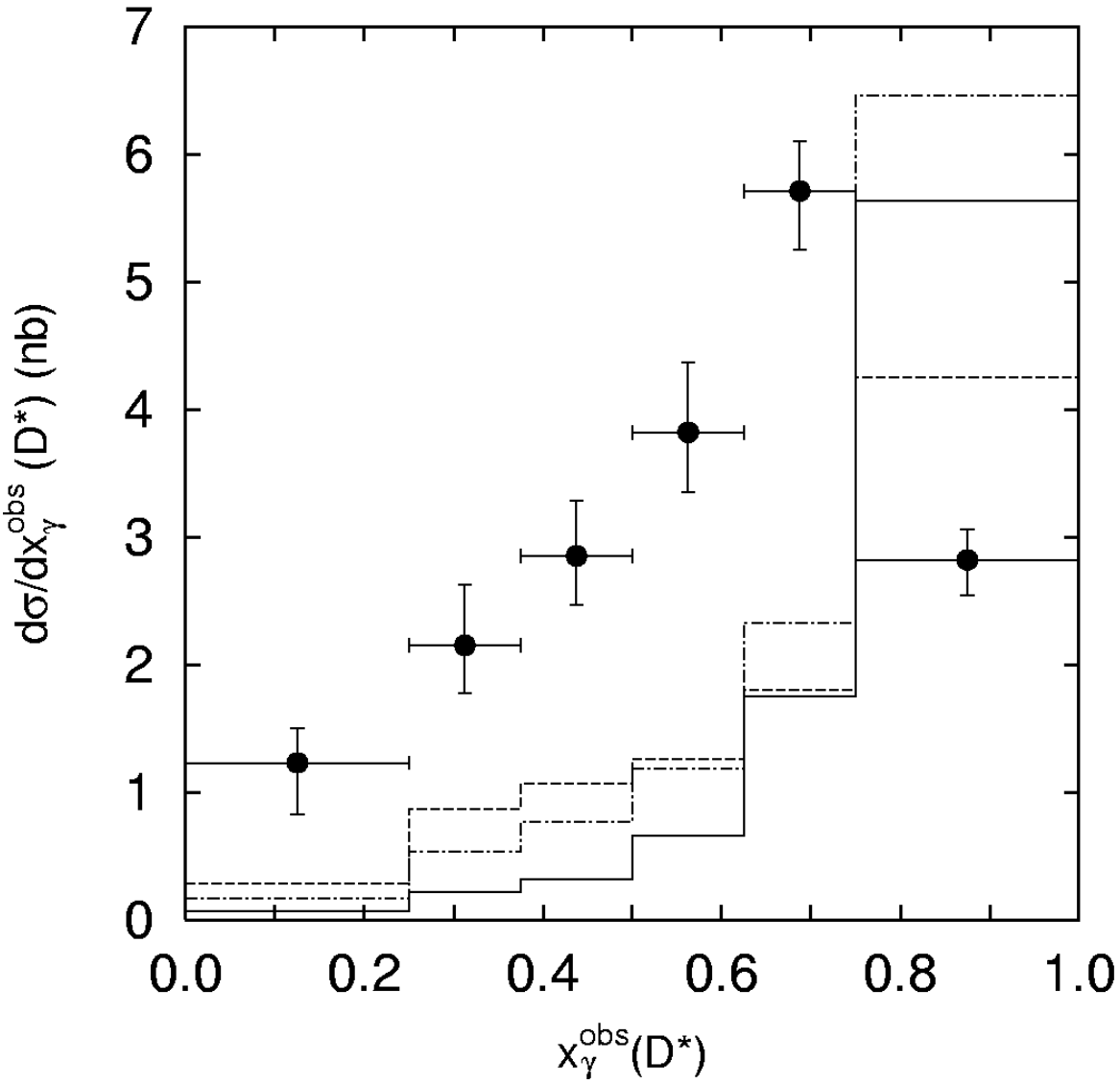

Figure 7: The $d\sigma/dx_\gamma^{\rm obs}(D^*)$ distribution of the associated $D^{*\pm}$ and jet production at HERA calculated in the kinematic range $Q^2 < 1$ GeV^2, $130 < W < 280$ GeV, $p_T > 3$ GeV, $|\eta| < 1.5$, $-1.5 < \eta^{\rm jet} < 2.4$ and $E_T^{\rm jet} > 6$ GeV. Notations of all histograms here are the same as in Fig. 1. The experimental data are from ZEUS [5].

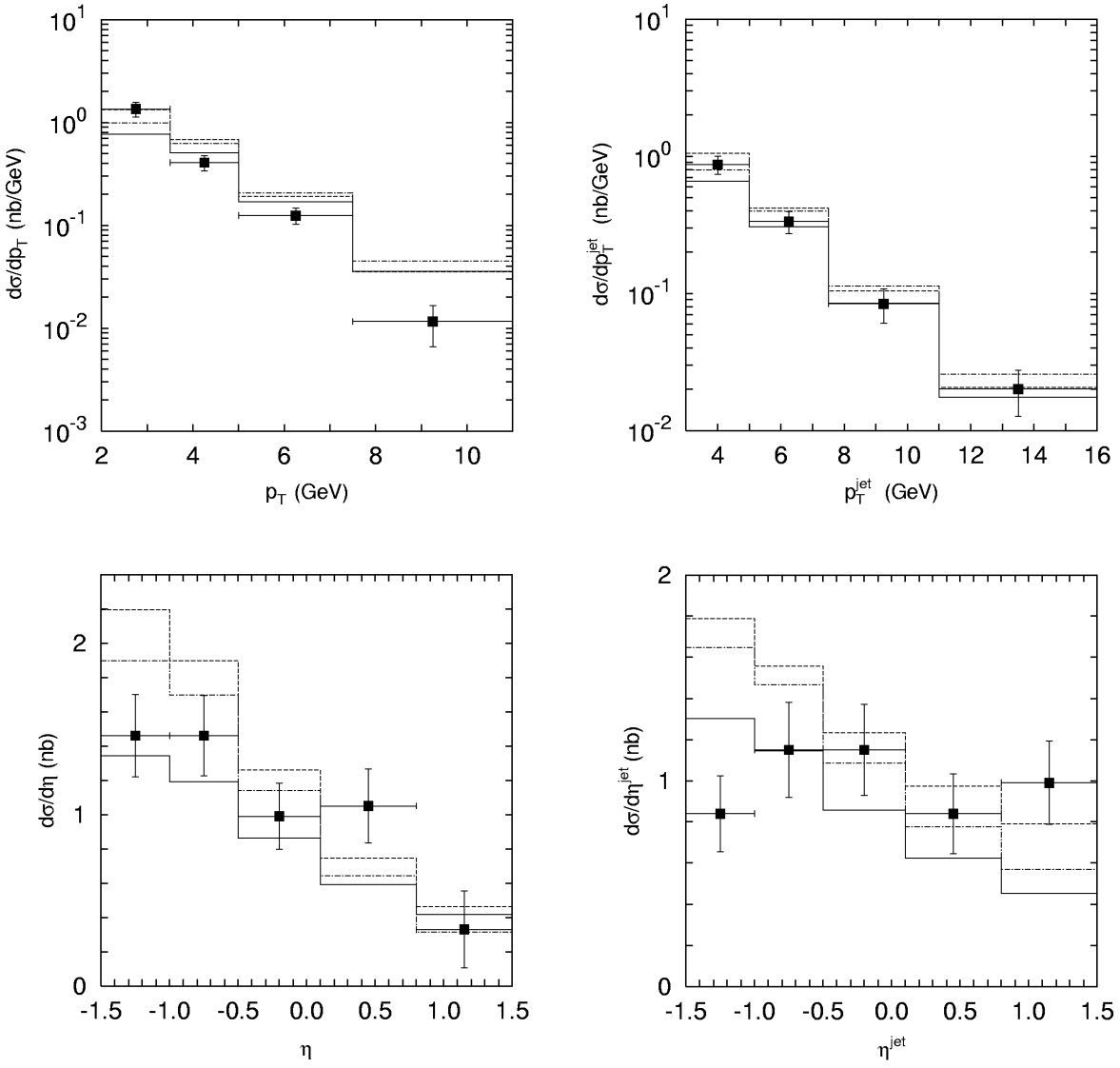

Figure 8: The differential cross sections of the $D^{*\pm}$ and untagged jet production at HERA calculated in the kinematic range $Q^2 < 0.01$ GeV^2, $0.29 < y < 0.65$, $p_T > 2$ GeV, $-1.5 < \eta < 1.5$, $p_T^{\rm jet} > 3$ GeV and $-1.5 < \eta^{\rm jet} < 1.5$. Notations of all histograms here are the same as in Fig. 1. The experimental data are from H1 [6].

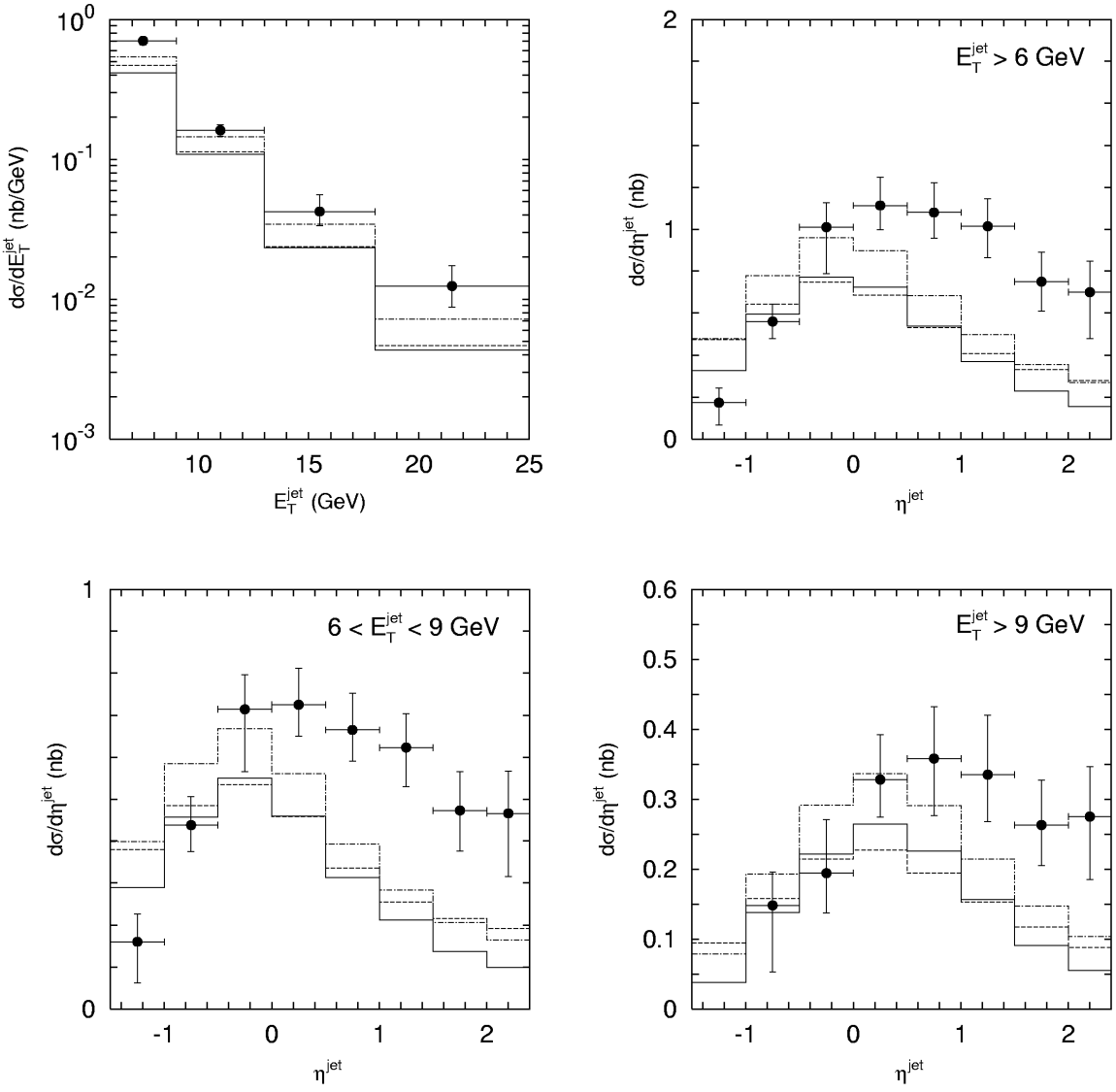

Figure 9: The differential cross sections of the $D^{*\pm}$ and untagged jet production at HERA calculated in the kinematic range $Q^2 < 1$ GeV^2, $130 < W < 280$ GeV, $p_T > 3$ GeV, $|\eta| < 1.5$, $-1.5 < \eta^{\rm jet} < 2.4$ and $E_T^{\rm jet} > 6$ GeV. Notations of all histograms here are the same as in Fig. 1. The experimental data are from ZEUS [5].

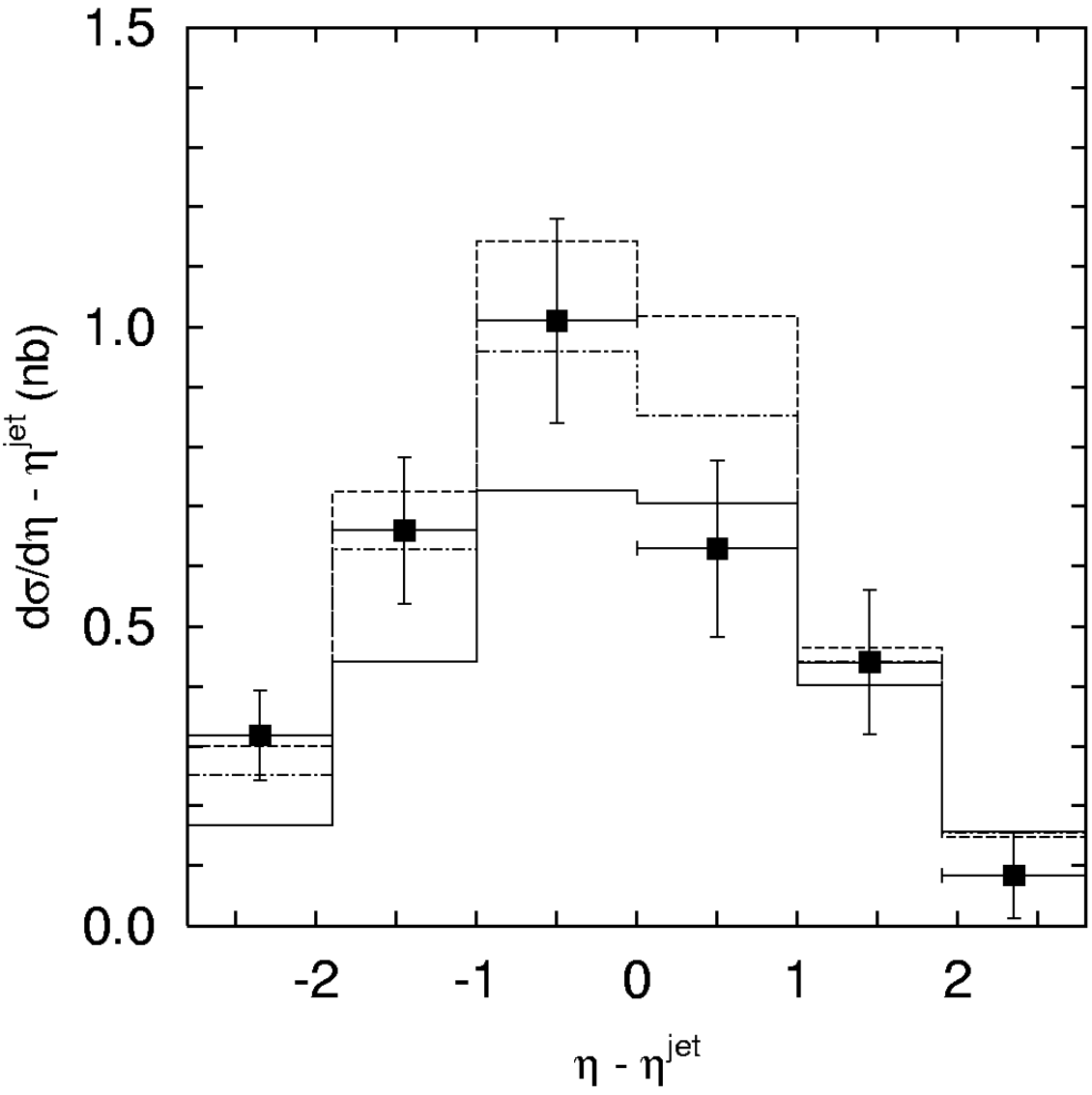

Figure 10: The cross section of the $D^{*\pm}$ and untagged jet production as a function of $\eta - \eta^{\rm jet}$ calculated in the kinematic range $Q^2 < 0.01$ GeV^2, $0.29 < y < 0.65$, $p_T > 2$ GeV, $-1.5 < \eta < 1.5$, $p_T^{\rm jet} > 3$ GeV and $-1.5 < \eta^{\rm jet} < 1.5$. Notations of all histograms here are the same as in Fig. 1. The experimental data are from H1 [6].

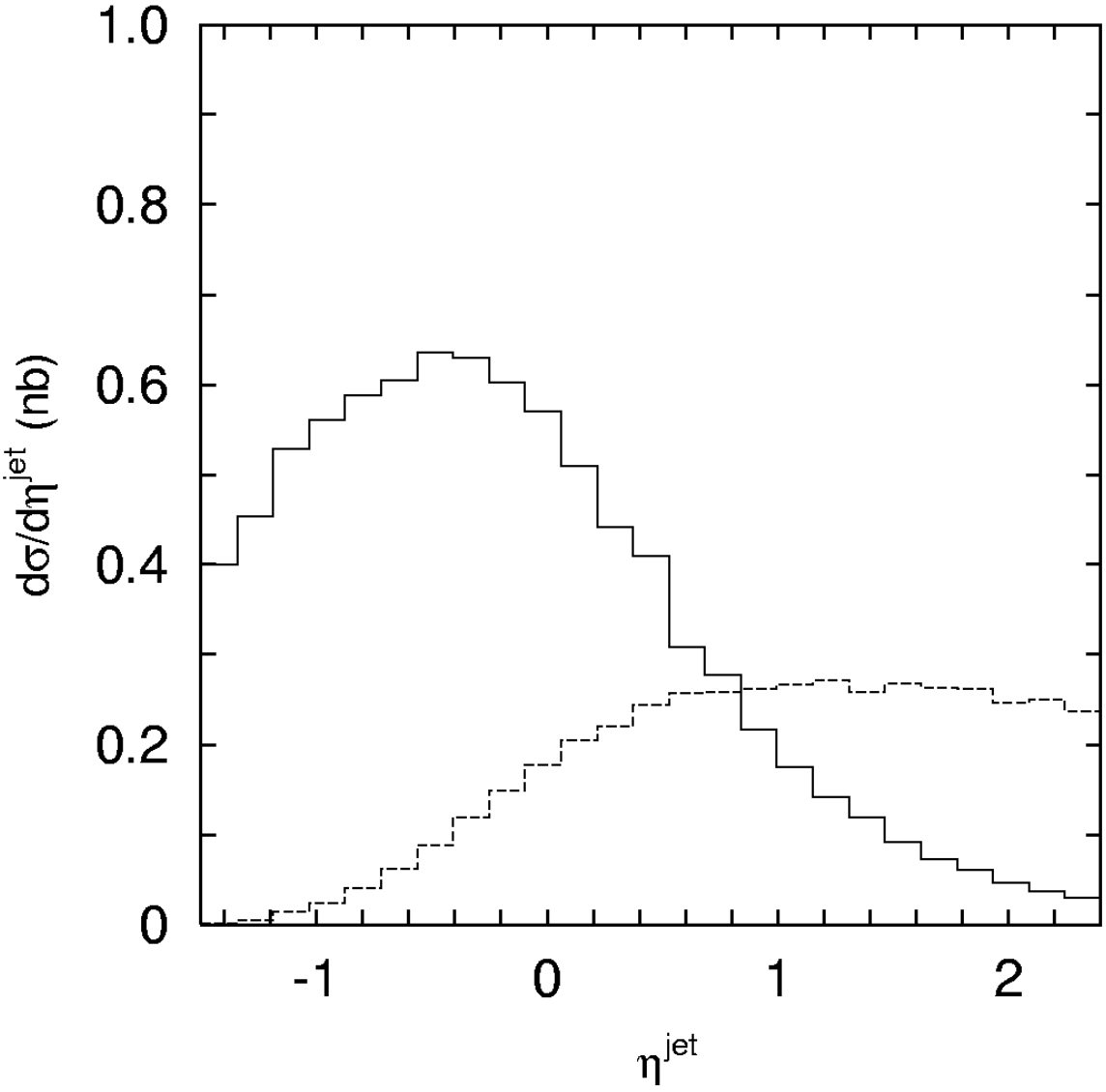

Figure 11: Direct (solid histogram) and resolved photon (dashed histogram) components of our central predictions of the differential cross section $d\sigma/d\eta^{\rm jet}$ calculated in the kinematic range $Q^2 < 1$ GeV^2, $130 < W < 280$ GeV, $p_T > 3$ GeV, $|\eta| < 1.5$, $-1.5 < \eta^{\rm jet} < 2.4$ and $E_T^{\rm jet} > 6$ GeV. The KMR unintegrated gluon densities in a proton and in a photon have been used.

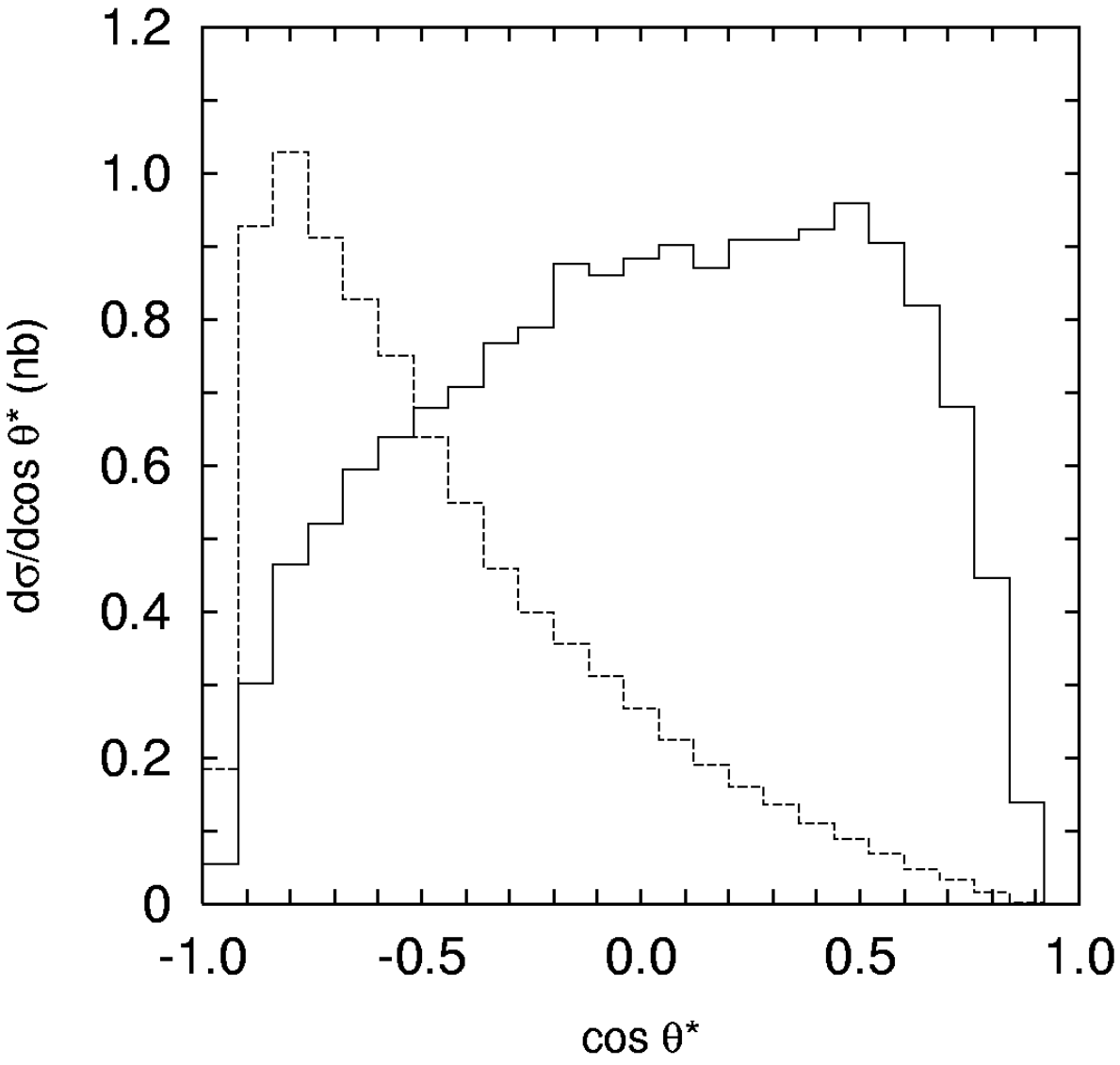

Figure 12: Direct (solid histogram) and resolved photon (dashed histogram) components of our central predictions of the differential cross section $d\sigma/d\cos\theta^*$ calculated in the kinematic range $Q^2 < 1$ GeV^2, $130 < W < 280$ GeV, $p_T > 3$ GeV, $|\eta| < 1.5$, $-1.5 < \eta^{\rm jet} < 2.4$ and $E_T^{\rm jet} > 6$ GeV. The KMR unintegrated gluon densities in a proton and in a photon have been used.

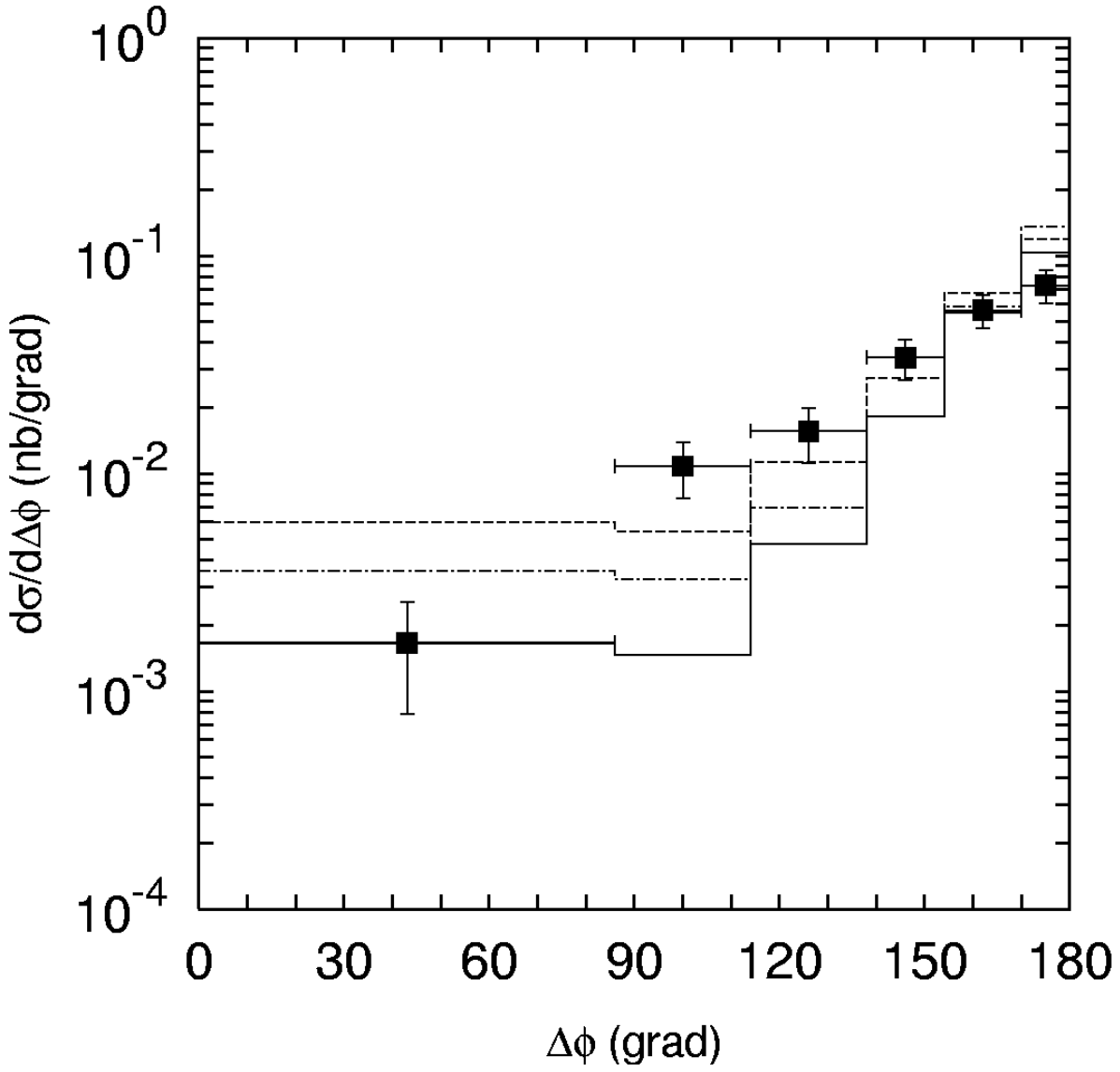

Figure 13: The cross section of the $D^{*\pm}$ and untagged jet production as a function of $\Delta\phi$ calculated in the kinematic range $Q^2 < 0.01$ GeV^2, $0.29 < y < 0.65$, $p_T > 2$ GeV, $-1.5 < \eta < 1.5$, $p_T^{\rm jet} > 3$ GeV and $-1.5 < \eta^{\rm jet} < 1.5$. Notations of all histograms here are the same as in Fig. 1. The experimental data are from H1 [6].

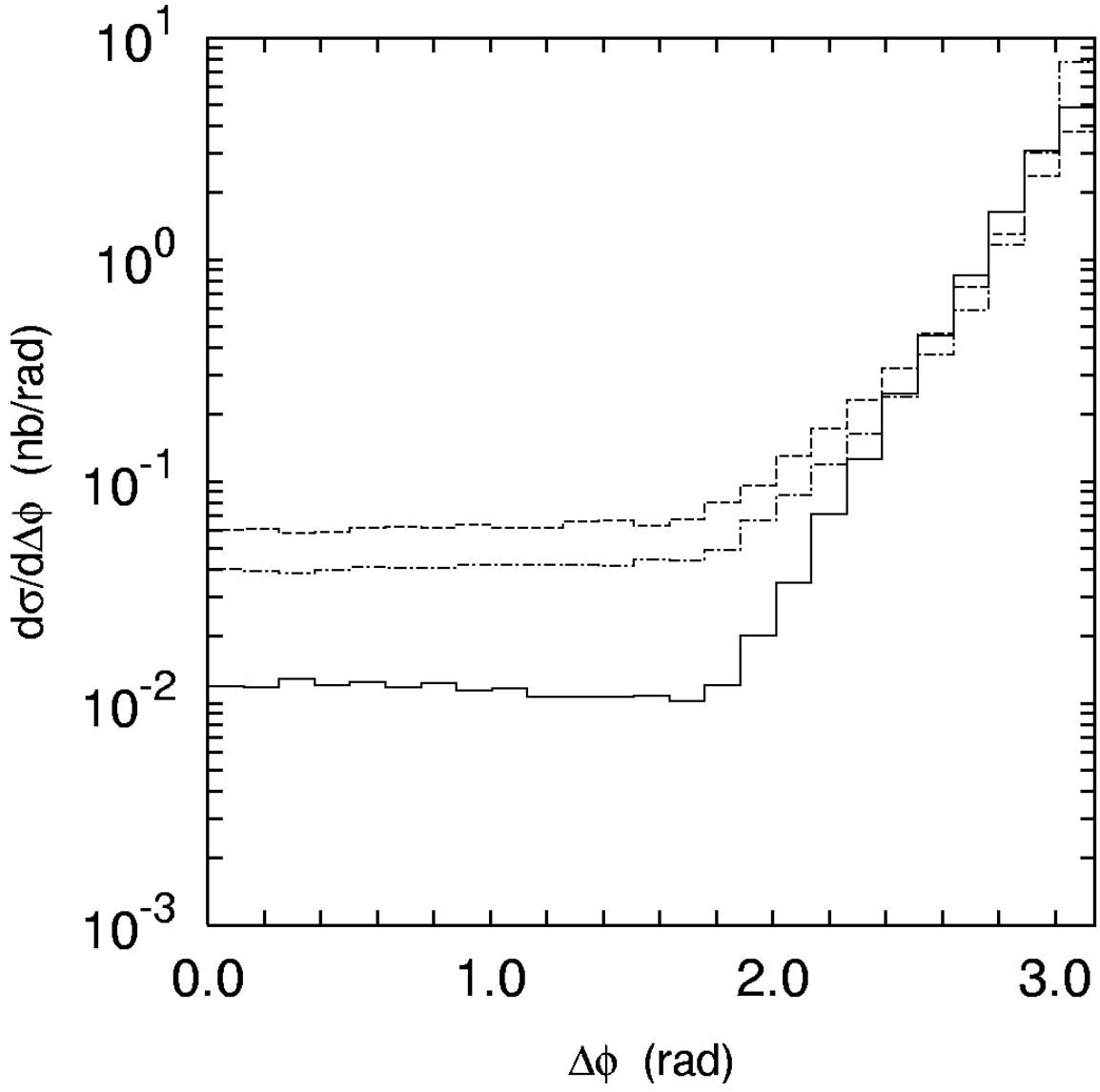

Figure 14: The cross section of the $D^{*\pm}$ and untagged jet production as a function of $\Delta\phi$ calculated in the kinematic range $Q^2 < 1$ GeV^2, $130 < W < 280$ GeV, $p_T > 3$ GeV, $|\eta| < 1.5$, $-1.5 < \eta^{\rm jet} < 2.4$, $E_T^{\rm jet} > 6$ GeV and $x_\gamma^{\rm obs}(D^*) > 0.75$. Notations of all histograms here are the same as in Fig. 1.

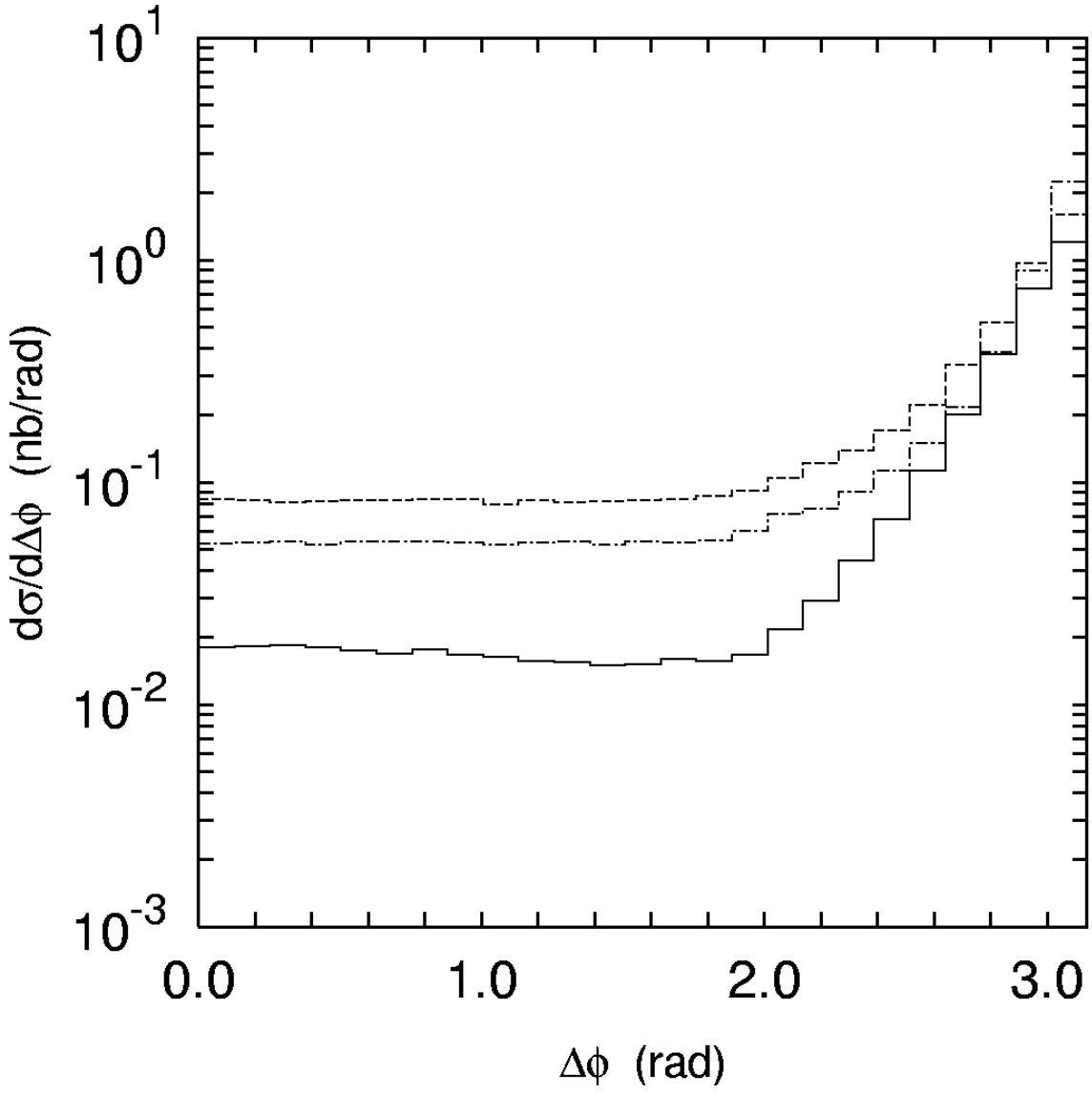

Figure 15: The cross section of the $D^{*\pm}$ and untagged jet production as a function of $\Delta\phi$ calculated in the kinematic range $Q^2 < 1$ GeV^2, $130 < W < 280$ GeV, $p_T > 3$ GeV, $|\eta| < 1.5$, $-1.5 < \eta^{\rm jet} < 2.4$, $E_T^{\rm jet} > 6$ GeV and $x_\gamma^{\rm obs}(D^*) < 0.75$. Notations of all histograms here are the same as in Fig. 1.